University of Stavanger

Faculty of Science and Technology

MASTER'S THESIS

Study program/ Specialization: Petroleum technology / Reservoir technology	Spring semester, 2012 Open
Writer: Joel Søvik	…… (Writer's signature)
Faculty supervisor: Svein M. Skjæveland External supervisor(s): Ingebret Fjelde	
Titel of thesis: Interactions between CO_2 and rock in heterogeneous reservoirs during CO_2 storage	
Credits (ECTS): 30	
Key words: CO_2 storage Reactive transport modelling CO_2 sequestration Heterogeneous PHREEQC	Pages: 75 + enclosure: 0 Stavanger,15/06/2012 Date/year

Acknowledgements

First I would like to thank my supervisor Dr. Ingebret Fjelde for his insight and directions throughout the course of the semester, and for defining the thesis wording.

I want to thank Ph.D candidate Alexandre Vilela for his generous help on various thesis related topics. Especially his help on the simulation software and general chemistry has been important.

I want to thank my faculty supervisor Prof. Svein M. Skjæveland for his discussion and guidance on the thesis.

Abstract

Reactive transport simulations of CO_2 storage in heterogeneous reservoirs are performed using the PHREEQC software by Parkhurst and Apello. When CO_2 dissolves in the pore water carbonic acid is formed. These aqueous species can react with the minerals in the reservoir and change the rock properties. Dissolving parts of heterogeneities may change vertical communication in the reservoir, increasing the storage capacity. The heterogeneities are modeled as low permeable layers in both the Frio formation at the Gulf of Mexico, and the Utsira formation in the North Sea. The results are heavily dependent on simulation boundary conditions and on how the pore waters are treated during the carbonation process. Calcite dissolution varying from only minor in one case to large amounts is evident of this. The dissolution of minerals in general seems to be highly dependent on pH, but apart from the calcite case, only minor dissolution occurred at the small time span of these simulations (<60 days). There was however observed minor precipitation of dawsonite.

Table of Contents

1 Introduction

Natural gas resources often contain a significant amount of CO_2 (Flett et al 2007). Removal of this species from the produced fluids is necessary both in processing of LNG and to meet market quality standards for petroleum products (Flett et al 2007). Also important is reducing CO_2 emissions to the atmosphere as a step in controlling global warming. One way of doing this is to capture the CO_2 and store it in deep sedimentary formations for long term sequestration (Xu et al 2011). The major options are depleted hydrocarbon reservoirs, saline aquifers and coal seams (Michael et al 2010). Out of these alternatives the saline aquifers have the largest storage potential globally (Michael et al 2010).

When injected CO_2 dissolves in the pore water there may be triggered various geochemical reactions (Gaus et al 2005). Environmental hazards may arise if the CO_2 reacts to such an extent with the host rock so that it is allowed to leak out into the atmosphere. During production from hydrocarbon reservoirs heterogeneities may affect the flow severely (Rahimpour-Bonab 2007). This is likely the case also for CO_2 inection and storage. Shale layers or other heterogeneities like stylolite's present in the reservoir may hinder vertical communication. So if vertical communication is important for the storage capacity, further knowledge on reactions between CO_2 and heterogeneities is desirable.

1.1 What to aim for

The aim of this thesis is therefore to establish further knowledge on reactions between CO_2 and heterogeneities in storage reservoirs. Since geochemical processes and reactions are of great complexity, reactive transport simulation is the necessary tool (Xu et al 2011). Other similar studies include (Xu et al 2005; Gaus et al 2005; Audigane et al 2006; Iglesias et al 2009; Liu et al 2011). The storage reservoirs that will be studied is Utsira in the North Sea, and Frio in the Gulf of Mexico. These are the same reservoirs studied by (Audigane et al 2006) and (Xu et al 2005). Mineral compositions and some other necessary simulation data will therefore come from these studies, which will for this reason sometimes be referred to as "source studies" for the Utsira and Frio simulations, respectively.

1.2 Plan of this thesis

In chapter 2 there will be given an introduction to CO_2 storage, where it's done and how it is stored. There will also be a chemistry section to show what chemical reactions one might expect from various minerals, and there will be an introduction to the simulation software used. This program is called PHREEQC and models a variety of chemical processes and reactions, including 1D transport and kinetic reactions.

In chapter 3 there will be presented and discussed all the data necessary to perform the simulations. This includes e.g. mineral surface areas and thermodynamic data. There will further be mentioned what are the exact scenarios to be studied, how brine will be carbonated and why it's performed in this exact way.

Next, in chapter 4 results and discussion from the simulations are presented. This includes both batch and transport modeling. Batch modeling is only performed to "create" the brines that will be used for the transport simulations. The transport simulations all involve letting a carbonated sandstone brine diffuse into a low perm layer called a heterogeneity. The last part of this section will be an "extra" result for Frio just for a comparison analysis.

Further, in chapter 5 is presented some proposals for further work, and chapter 6 is a summary of the conclusions from the discussion in chapter 4. At last chapter 7 contains literature references.

2 BACKGROUND

2.1 Examples of Storage Sites and Projects

The Sleipner project is shown in the figure below

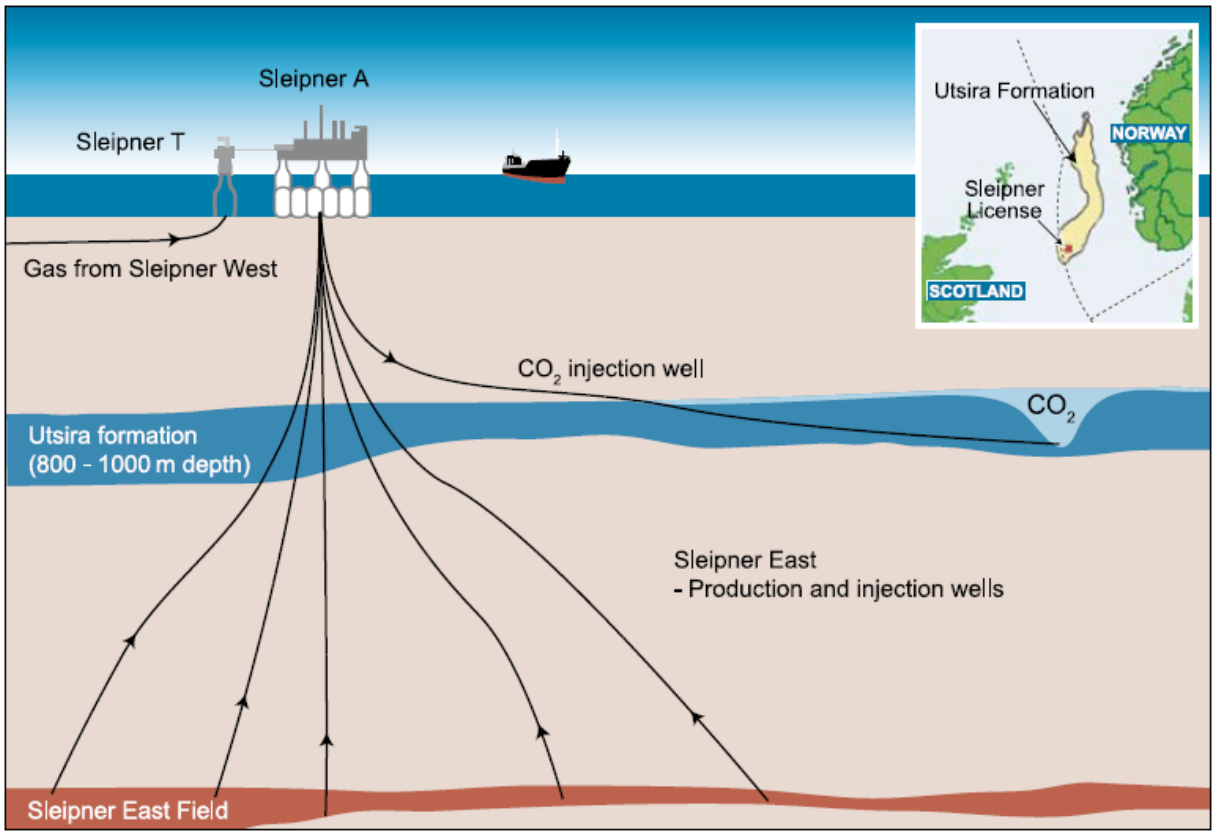

Figure 2.1: Sleipner project with CO_2 injection. Figure from (IPCC 2005)

The Sleipner project stores CO_2 in a saline aquifer, the Utsira formation, near the Norwegian west coast (IPCC 2005). The project has stored CO_2 from the Sleiper natural gas field since 1996, and the storage potential is estimated to be 1-10 gigatonnes CO_2 (IPCC 2005). By 2008 there has been stored 10 million tonnes (Shukla 2010). The utsira formation is a 200m-300 m thick sandstone at a depth of about 1000 m (seen in Figure 2.1), with shale as caprock (Shukla 2010).

The Weyburn project launched in the year 2000 in Canada, injecting CO_2 from the Dakota Gasification company facility into the Midale carbonate reservoir of the Weyburn field (Shukla 2010). This is an oilfield, so the injection is combined storage and EOR purposes. 20 mega tonnes of CO_2 is estimated to be stored in the field.

A project named In Salah in Algeria injects CO_2 both for storage and as an EOR fluid into a 20 m thick sandstone where methane is produced. The reservoir is located at about 1800 m depth, near the Krechhba gas field.

Another project started in 2007 in Australia, the Otway Basin Pilot project (Shukla 2010). The reservoir is again sandstone, and the caprock a mudstone. CO_2 from a proximity gas well is being injected into a saline aquifer, the Naylor field in the Otway Basin. The goal of the project was to inject 100 000 tonnes of CO_2 over the course of two years.

All of the mentioned projects use technology for monitoring the CO_2 distribution in the reservoir with time (Shukla 2010). This is important in ensuring that no leakage is taking place.

2.2 Storage Mechanisms

There are four main mechanisms behind geological CO_2 sequestration in aquifers (Shukla 2010). These are the trap and seal combo, mineral precipitation, dissolution in the water phase, and capillary trapping (Shukla 2010).

2.2.1 Trap and seal

The trap and seal combo is keeping the CO_2 plume (gaseous phase) from leaving the reservoir due to buoyancy forces (Shukla 2010). There will always be some degree of diffusion of CO_2 through this caprock, but with a sufficiently tight caprock this is an extremely slow process (Shukla 2010). The injection of CO_2 might cause an acid environment, and minerals could start reacting with the caprock at increased pace, damaging the seal (Shukla 2010). Geochemical models can be used to predict the degree of which the caprock is getting teared.

2.2.2 Dissolution mechanism

The dissolution mechanism occurs once the injected CO_2 contacts formation water. When CO_2 is dissolved in water it no longer exists as a separate phase, so that buoyancy forces don't drive it towards the seal (IPCC 2005). Solubility of CO_2 in water depends on temperature, pressure and salinity (Shukla 2010). Increasing amounts of dissolved CO_2 in water will increase its density. This in turn will create currents bringing water with a low

amount of dissolved gas towards the CO_2 plume - water interface, thereby allowing further dissolution (Shukla 2010).

2.2.3 Mineralization

Mineralization occurs whern the carbon element of CO_2 is stored as a solid phase in the reservoir due to chemical reaction (Shukla 2010). The reaction may be directly between gaseous CO_2 and the sediment or between dissolved CO_2 and minerals in the water phase. The mineralization storage mechanism is a very slow process, and very complex. Thousands of year may be required to complete the process (IPCC 2005).

2.2.4 Capillary Trapping

Capillary trapping occurs after the injection process is finished, and the CO_2 plume starts migrating upwards due to buoyancy (Shukla 2010). The water imbibes behind the moving plume, trapping CO_2 in the form of immobile bubbles. These bubbles are unable to move through the pore throats due to capillary forces.

2.3 Chemistry

2.3.1 Brine – CO_2 Interaction

A simplified version of CO_2 dissolution in water is presented below, all by (Dickson and Goyet 1994).

First the equation C-1 represents the phase change of gaseous CO_2 into aqueous CO_2.

C-1 $$CO_2(g) \rightleftarrows CO_2(aq)$$

Equation C-2 represents the hydrolysis of aqueous CO_2, creating the carbonic acid.

C-2 $$CO_2(aq) + H_2O \rightleftarrows H_2CO_3$$

The distinction of $CO_2(aq)$ and H_2CO_3 is made, and they are usually gathered in a common term as

C-3 $$CO_2(aq)^* = CO_2(aq) + H_2CO_3$$

or, if preferred, as

C-4 $$H_2CO_3{}^* = CO_2(aq) + H_2CO_3$$

It could be mentioned here just to give a picture that at 25°C the abundance of $CO_2(aq)$ is 600 times larger than H_2CO_3 (Appelo 2005).

Further reaction into bicarbonate and carbonate is shown in equation C-5, and C-6, respectively.

C-5 $$CO_2(aq)^* \rightleftarrows H^+ + HCO_3{}^-$$

C-6 $$HCO_3{}^- \rightleftarrows H^+ + CO_3{}^{2-}$$

2.3.2 Mineral Dissolution (and precipitation)

Calcite will get a special mention here since it will be of special importance in the result section. There are three dissolution reactions for calcite (Appelo and Postma 2005)

C-7 $$CaCO_3 + H^+ \rightleftarrows Ca^{2+} + HCO_3{}^-$$

C-8 $$CaCO_3 + H_2CO_3{}^* \rightleftarrows Ca^{2+} + 2HCO_3{}^-$$

C-9 $$CaCO_3 + H_2O \rightleftarrows Ca^{2+} + HCO_3{}^- + OH^-$$

These equations are dominant in each their pH interval, the first equation at pH < 3.5, the second for pH <7, and the last equation for pH > 7 (Appelo and Postma 2005).

For the rest of the minerals considered, dissolution and precipitation reactions used by PHREEQC are presented in the following table 1, and is found in the phreeqc.dat database.

Table 2.1: Dissolution / Precipitation reactions in PHREEQC. The reactions are from the phreeqc.dat databse.

Mineral	Equation	Reaction
Quartz	C-10	$SiO_2 + 2H_2O \rightleftarrows Si(OH)_4$
Albite	C-11	$NaAlSi_3O_8 + 8H_2O \rightleftarrows Na^+ + Al(OH)_4^- + 3Si(OH)_4$
Anorthite	C-12	$CaAl_2Si_2O_8 + 8\,H_2O \rightleftarrows Ca^{2+} + 2\,Al(OH)_4^- + 2\,Si(OH)_4$
K-feldspar	C-13	$KAlSi_3O_8 + 8\,H_2O \rightleftarrows K^+ + Al(OH)_4^- + 3\,Si(OH)_4$
Illite	C-14	$K_{0.6}Mg_{0.25}Al_{2.3}Si_{3.5}O_{10}(OH)_2 + 11.2H_2O \rightleftarrows 0.6K^+ + 0.25Mg^{2+} + 2.3Al(OH)_4^- + 3.5Si(OH)_4 + 1.2H^+$
Hematite	C-15	$Fe_2O_3 + 6H^+ \rightleftarrows 2\,Fe^{3+} + 3\,H_2O$
Pyrite	C-16	$FeS_2 + 2\,H^+ + 2\,e^- = Fe^{2+} + 2\,HS^-$
Alunite	C-17	$KAl_3(SO4)_2(OH)_6 + 6\,H^+ = K^+ + 3\,Al^{+3} + 2\,SO_4^{2-} + 6H_2O$
Chlorite(14A)	C-18	$Mg_5Al_2Si_3O_{10}(OH)_8 + 16H^+ = 5Mg^{2+} + 2Al^{3+} + 3Si(OH)_4 + 6H_2O$
Magnesite	C-19	$MgCO_3 \rightleftarrows Mg^{2+} + CO_3^{2-}$
Dawsonite	C-20	$NaAlCO_3(OH)_2 + 3H^+ \rightleftarrows Al^{3+} + HCO_3^- + Na^+ + 2H_2O$
Ankerite	C-21	$CaFe(CO_3)_2 + 2H^+ \rightleftarrows Ca^{2+} + Fe^{2+} + 2HCO_3^-$
Kaolinite	C-22	$Al_2Si_2O_5(OH)_4 + 6\,H^+ \rightleftarrows H_2O + 2\,Si(OH)_4 + 2Al^{3+}$
Na-montmorillonite	C-23	$Na_{0.33}Mg_{0.33}Al_{1.67}Si_4O_{10}(OH)_2 + 10.68\,H_2O \rightleftarrows 0.33Mg^{2+} + 0.33\,Na^+ + 1.67\,Al(OH)_4^- + 4\,Si(OH)_4 + 0.68\,H^+$
Calcite	C-24	$CaCO_3 \rightleftarrows Ca^{2+} + CO_3^{2-}$
Siderite	C-25	$FeCO_3 \rightleftarrows Fe^{2+} + CO_3^{2-}$
Muscovite	C-26	$KAl_3Si_3O_{10}(OH)_2 + 10H^+ \rightleftarrows K^+ + 3Al^{3+} + 3Si(OH)_4$
Dolomite	C-27	$CaMg(CO3)_2 \rightleftarrows Ca^{+2} + Mg^{+2} + 2\,CO3^{2-}$

2.4 Geochemical Modeling in PHREEQC

PHREEQC by Parkhurst and Apello is a computer program for calculation of various geochemical reactions and transport mechanisms in aqueous settings (Parkhurst and Appelo 1999). Both equilibrium and kinetic modeling is possible in either a batch or 1D transport setting.

2.4.1 1D Mass Transport: Advective and Diffusive

For the 1D transport, both diffusion alone, and advective-diffusive transport is possible. (Parkhurst and Appelo 1999) Advection is simply any particles following the bulk motion of a medium, while diffusion is mass transport due to concentration gradients. E.g. rupturing a

helium balloon will cause the helium particles to spread out and distribute itself uniformly across the room. This is caused by random movements in the molecules, called Brownian motion and makes the molecules bounce into each other. Higher kinetic energy of the molecules (higher temperature) means these collisions happen at a higher pace, enhancing the diffusion process. Advection, on the other hand, happens when any substance that can be contained by a medium is moved simply because the medium moved. E.g. calcium may be carried down a river just following the water stream.

In PHREEQC, the advective transport is performed by first specifying a grid consisting of single calculation points in a column (Parkhurst and Appelo 1999). Every cell is attributed a pre-defined solution of any size. Also, in each of these grid cells one may specify mineral assemblages that may react either kinetically or be assumed to be in equilibrium with the solution in the same cell. But there are a variety of options here, e.g. surface sorption sites and solid solutions are two of them. An infilling solution is then defined, and also a time step length. After each time step, advection is performed by successively shifting the solution located at cell n over to cell n+1. That is, every solution is shifted one grid cell in the forward direction. There is also defined an infilling solution, which for every time step will fill in the cell at the end of the column, the first cell. At the other endpoint, the solution in the last cell is shifted out of the column. This whole process is then repeated for any chosen number of steps.

For diffusion calculations, PHREEQC simply performs a number of mixing steps where the solution located at grid cell n is to some specified degree mixed with solution n+1 and n-1. If one chooses a setting that allows both advective and diffusive mass transport, then for every advective shift performed (which is user specified) a number of diffusive mixes are performed for each of these. Exactly how many is determined by PHREEQC so that the von Neumann Criterion for avoiding oscillations is fulfilled (Parkhurst and Appelo 1999).

In figure 2.2 are presented a simplified sketch that should display more clearly how PHREEQ works, and what have been done in this study. Some of the concepts that were just described in a rather abstract manner will to some degree be echoed in this section, but in a more concrete context, closely tied to the figure.

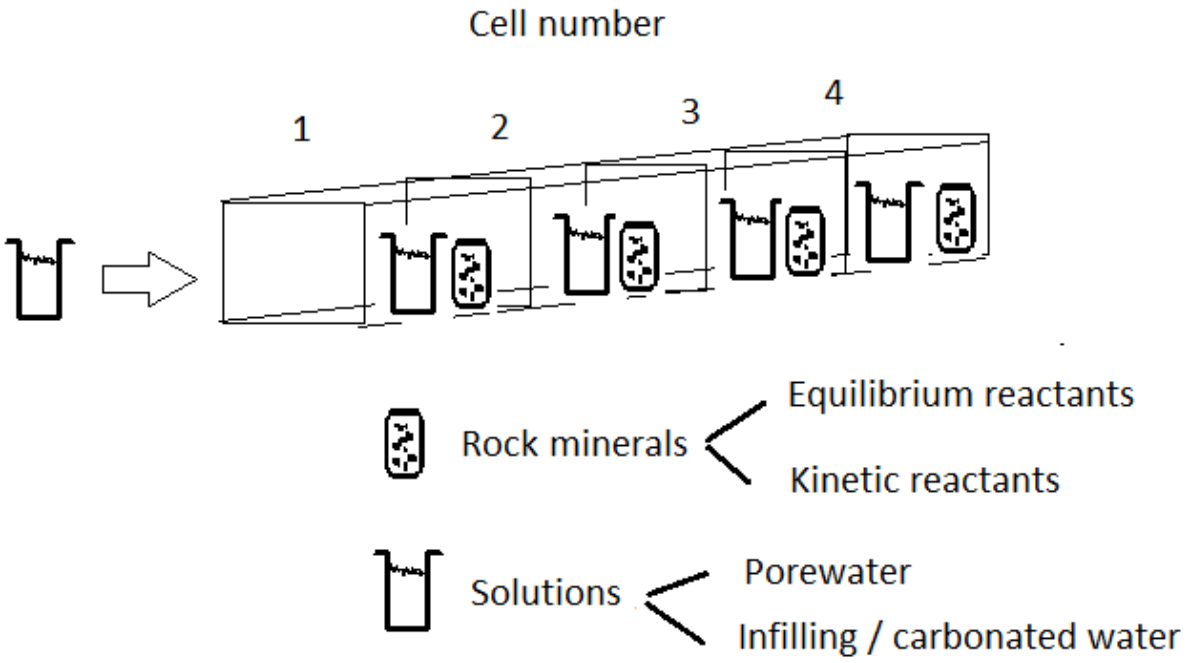

Figur 2.2: Schematic representing the transport process in PHREEQC

First, a remark on the figure. The grid has been shown in 3D for simplicity, but PHREEQC only models 1D transport. But the principle remains the same.

So one defines an arbitrary amount of grids that one chooses to contain an initial solution and some minerals that represents the reservoir column of interest. There are also a lot of other options for more advanced users, as mentioned, like surface sorption sites and solid solutions, with more. These are not used in the following study though.

Further, the minerals dissolution/precipitation rates can either be governed by a user specified rate equation, or can be taken to be an equilibrium reactants, as shown in the figure. This means that they will always be assumed to be in equilibrium with the solution, so no rate equation is required in this case.

The initial solutions are then specified, one for every grid cell. In this study all the solutions in the column are equally defined. They are equal to a brine that is in equilibrium with the columns minerals. As is described later in this study, the column studied will be low perm layers. So the brine is then just the brine that would be in equilibrium with this columns sediment minerals. In section 2.4.3 it is explained that these solutions are found by batch modeling.

There is also a solution called the infilling solution. This is discussed later in this study, but is going to be sandstone pore water that is carbonated by a high pressure CO_2 gas phase. This is discussed in detail in section 3.6. And as already mentioned, the infilling solution may advect into the column, or diffuse or both. In the present study, only diffusion will be the case since the column will be low perm layers.

2.4.2 Numerical Dispersion

Transport simulations are based on solving equations involving exact differentials (Parkhurst and Appelo 1999). These terms are not known exactly, and must be replaced by finite difference approximations. This causes a calculation error called numerical dispersion, and may be reduced to a minimum by using adequately small grid size.

The common approach is to start out with a coarse grid size, fining it in steps until the simulation results converge towards a common value, and more fining of the grid has diminishing value. The prize is the increased simulation runtime. Numerical dispersion cannot be reduced completely though, and will therefore be a necessary limitation in the results.

2.4.3 Batch modeling

The contrary to transport modeling is batch modeling. This just means that there is no mass transport to or from the system. Batch modeling in the context of this study is only performed prior to the transport calculations. Since for transport calculations one will have solutions defined initially at every grid cell, as well as an infilling solution, the specification of these results come from batch calculations.

2.4.4 Ionic strength and activities

The PHREEQC developers report that PHREEQC use a few different approaches in calculating activity coefficients (Parkhurst and Appelo 1999). E.g. major cations have been fitted using chloride salts, so activity coefficients in chloride dominated solutions are expected to be relatively accurate. For ion pairs and complexes the Davies equation is used, which is also based on empiric data. So exactly what ionic strength is too large for calculations is not entirely clear. It is suggested that this value is somewhere between 0,1 and 2, and that for solutions with large amounts of complexing, values of > 0,5 is suspect. There is, however, no suggestion of what degree of complexing is considered “large”.

Checking a few random solutions from the present study reveals ionic strengths to vary roughly between 0,5 and and up to 1.2. But they could be both smaller or greater. However, the amount of chloride in these solutions is quite large, about 1 molal, which should brighten this side of the modeling slightly.

2.4.5 Gas Phase Modeling

In high pressure gases the partial pressures may give a poor estimate of chemical potentials. This can be compared to using concentrations instead of activities in non-diluted solutions. Therefore fugacity is used, which is an effective pressure that replaces the partial pressure. This is analogous to activities, which are effective concentrations for solutes.

PHREEQC gas phase modeling is based on the ideal gas law (Soong et al 2003). In the calculations, CO_2 will be the only component present. Therefore the partial pressure is equal to its total pressure, which will be the fugacity. The pressure is selected to be fixed through the calculations. The initial volume is set to any arbitrary value that ensures that the ideal gas law used by PHREEQC finds an initial amount of moles that are big enough to not be totally dissolved during the run. I.e. an open system will be assumed, as will be described in section 3. It basically just means that the brine carbonation process won't run out of CO_2, which assumes that it will be present in abundance in the reservoir. The only simulation where gas phase modeling is actually used is in the batch modeling calculations.

Below is presented CO_2 fugacity coefficient correlations, by (Marini 2006)

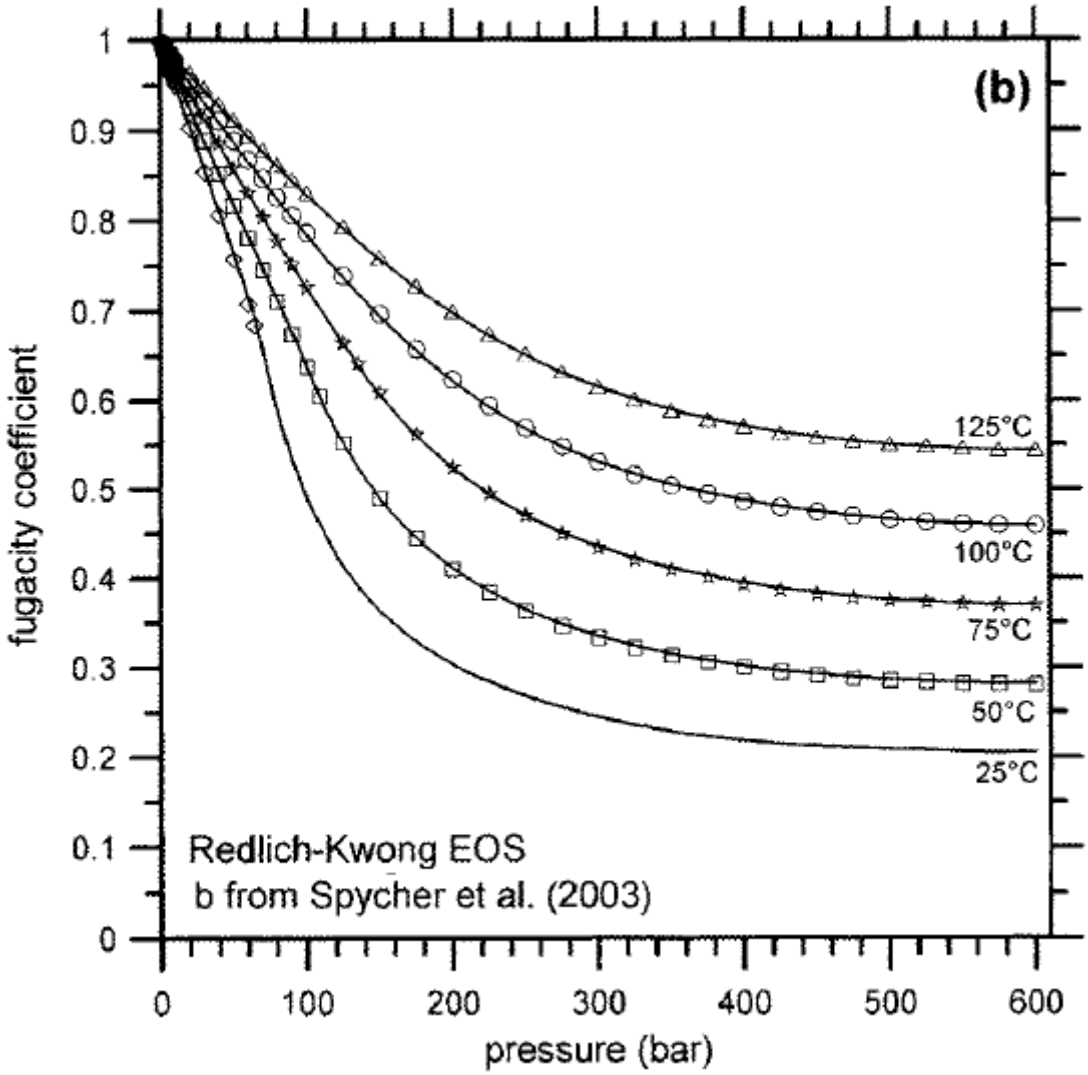

Figure 2.3: Fugacity coefficient vs pressure. Figure from (Marini 2006)

This figure will be used to calculate fugacities for the Frio

2.4.6 Boundary Conditions

There are three possible boundary conditions one can use in PHREEQC. These are closed, flux and constant.

The closed boundary condition just means that this is a no-flow boundary, i.e. there will not occur any mass transport through this boundary.

The constant boundary condition means that for every time step calculated, the concentration of all species at this point is updated to its initial concentration. This is going to be important in this thesis, and will be discussed later. The consequence here is that the infilling solution will act like a “sink” or “pump” for some species if the concentration difference across the boundary is large.

The last boundary condition is called flux. This means that the concentration at the boundary is changed continuously through the whole simulation. E.g. if the infilling solution has calcium diffusing into it, the concentration will increase with time and not "reset" like the constant boundary condition would.

If one were to choose the flux boundary condition, there would be another dimension to this, namely the size of the infilling solution. This would determine to what extent the infilling solution would be affected by diffusion. The constant concentration boundary condition is in this sense only a flux boundary condition with an infinitely large size of the infilling solution, meaning it won't be affected by mass transport.

In this thesis, the constant boundary condition is chosen at the inlet side (x=0), whereas the flux boundary condition is chosen at the opposite end (x=L). But since there is not defined any sediment nor any solution further than this end boundary, its effectively going to be a closed boundary condition.

The most impacting choice of boundary condition is still at the inlet. This is going to be quite evident in the results, and will therefore be discussed later.

2.5 Mineral Kinetics

2.5.1 Mineral Kinetic Rate Equation and Rate Constant

For mineral dissolution and precipitation, the following rate equation is used

E-1 $$r_{m=}k_m * A_m * a_{H+}^n [(\frac{Q_m}{K_m})^u - 1]^v$$

where r is the dissolution/precipitation rate, A is the specific reactive surface area per kg H_2O, k is the rate constant, a_{H+} is the proton activity, n is the reaction order, K is the equilibrium constant, Q is the reaction quotient, m is the mineral index, u and v are experimental constants often taken to be equal to one (Iglesias et al 2009). This is also done in the present study.

A limitation here is the reative surface area per kg water, which is treated as a constant. Since the surface area per kg water changes during the simulation, this is not going to be accurate. It can be close to accurate for minerals showing only small will to dissolve / precipitate, but in case of highly reactive minerals this is not going to be accurate throughout the simulation.

The temperature dependent kinetic rate constant is calculated by the following equation

E-2 $$k = k_{25} * \exp[\frac{-E_a}{R} * (\frac{1}{T} - \frac{1}{298.15})]$$

where k_{25} is the rate constant at 25°C, E_a is the activation energy, and T is the absolute temperature (Iglesias et al 2009).

2.5.1 Mineral Surface Areas

Mineral dissolution rates depend on the area of mineral exposed at the solid-liquid interface, namely the wetted surface area, also called the reactive surface area (Marini 2006). This parameter is highly uncertain and also very sparse in the literature. There are two ways of determining this parameter, gas sorption on mineral surfaces (BET method) and calculations based on ideal geometry of mineral grains (Marini 2006).

As further described by (Marini 2006), the BET (by Brunauer, Emmet and Teller) method is performed in two steps; first the surface of any fine grained solid reactant is heated to desorb all previously adsorbed gases. The sample is then exposed to a gas, usually nitrogen or krypton, and the total amount then adsorbed is measured.

The assumption is then that exactly a single layer of gas is adsorbed to the surface. Since these gases have approximately the same diameter as water, the area that will be exposed to water molecules at the wetted surface will be close to that as for the gases in the experiment.

The geometry approach is the one used for all the surface areas in this study. The values are taken from several papers, but they are reported by (Xu et al 2005; Audigane et al 2006) to origin from (Sonnenthal and Spycher 2001). Their calculations were made based on mineral grains modeled as a cubic array of truncated spheres.

The geometric approach gives questionable results both because minerals deviate from ideal geometric shape, and also it does not take into account that only the wetted surface takes part in reactions. That is, only the part of the surface exposed to liquid water should be considered reactive. This can be corrected multiplying by a surface roughness factor, defined either as the “true” - or as the BET – surface, divided by the ideal geometric surface. Since the BET surface should be a close approximation to the “true” water wetted surface, this would be the favorable approach.

These roughness factors are, however, quite dependent on grain shape and also the extent to which they have been exposed to weathering, which is usually unknown. These values are also not very abundant in the literature. For these reasons they are not used in this study, and it is therefore assumed that the geometric surface area is a good enough measure.

Also, in real reservoirs where minerals coexist there are also additional factors that affect the reactive surface area, like for example coating.

And as a last limitation, the kinetic rate parameters in the literature are usually normalized to BET surfaces, so this is also an error source in using the geometric surface area.

This is an overview on the topic, and is described in more detail by (Marini 2006).

3 SIMULATION DATA AND METHODS

3.1 Secondary minerals

Secondary minerals are the minerals not present initially, but are allowed to precipitate out of solution during the simulation. The process of determining the secondary minerals is described by (Gaus et al 2005).

The way it's done is as follows. The secondary minerals are determined by assuming thermodynamic equilibrium between the primary minerals and pore water carbonated through a high pressure CO_2 phase. PHREEQC then serves the saturation indices of all the minerals present in the database. The secondary minerals are now selected among the minerals found to have positive saturation indices. However the ones that are experimentally or empirically known to not form under these conditions are not considered.

This approach has its limitations, because some minerals may precipitate and re dissolve in the course of time before equilibrium is reached (Gaus et al 2005). So already a proposal of future work may be suggested, namely sensitivity on secondary minerals. This is also stressed in (Gaus et al 2005).

3.2 Neutral and acid catalyzed kinetic rates

In this section it will be discussed a way of doing the simulations that is chosen to not be done, as explained later. The idea is to use rates corresponding to a pH of around 7 in the batch modeling to create the heterogeneity pore water. And next using rates corresponding to a acid catalyzed environment for the transport calculations, which will be the correct approach nearly the whole simulation (with the exception of a very small amount of time at the beginning of simulation when no severe diffusion of protons have taken place). But this is not done, as will be discussed here.

So to be a bit more thorough on this topic. There are a few general steps for every simulation. Two of them are considered here to discuss an issue on kinetic rate data. The first step consists of running a batch calculation to create pore water equilibrated with the sediment. This will be present initially in the pores in the column of rock studied. The pH in this case is reported from other similar studies, like (Gaus et al 2005; Xu et al 2005; Iglesias et al 2009) to roughly be somewhere around 7. Therefore, ideally, these simulations should use rates that correspond to a neutral mechanism, as described in (Palandri and Kharaka

2004). The pH interval defined to be within this “neutral region” are not the same for every mineral, they are quite variable, but roughly one can say they lie around a pH of 7.

The other step is the transport step, where CO_2 saturated brine is brought into the column of rock by diffusion or diffusive-advective mass transport. Now the pH will drop considerably, dependent on how much time has passed and how big the column of rock is set to be. In the following simulations the pH will usually drop into roughly the 4,5 to 5,5 region within a relatively short time. Therefore, for this transport step there should be used mineral kinetic rates according to an acid mechanism (acid catalyzed), also described in (Palandri and Kharaka 2004).

Though this approach sounds like a quite rigorous approach, it regrettably introduces quite a few difficulties, and had to be abandoned.

To mention just a few of these difficulties, the neutral mechanism rates cause the pH in Frio to increase to value of about 10 in the batch simulation. This is quite far from what is found in both Frio by (Xu et al 2005) and e.g. at Utsira by (Audigane et al 2006), where values are close to 7. One therefore has to introduce a low pressure CO_2 gas phase just to keep the pH within a reasonable range. This was also done in the (Xu et al 2005) study on Frio, just to keep the pH within observed field ranges. Now from here the problems split into two directions.

One is that even though one use this gas phase approach and are able to keep the pH reasonable in the batch calculations, one cannot keep this low pressure gas phase present when one runs the transport simulations. The reason is that when the pH eventually decreases because of the transport, the allowed presence of this gas phase may cause newly formed – or transported - CO_2 to vaporize out of solution. The pressure in this “dummy” gas phase is very low (a fraction of an atmosphere), so vaporization could easily happen during the transport simulation. This would not be representative for a high pressure reservoir, allowing the dissolved CO_2 to leave the solution.

Another problem is that if the columns pore water is created assuming equilibrium with sediment governed by neutral mechanism rates, and the transport simulation will use acid mechanism rates; there would not be equilibrium between the pore water and the sediments at the onset of the transport simulation. This problem will of course vanish at the time the transport has decreased the pH into the acid region. This will not happen instantly though. And the impression is that even very small timescales could change the pore water chemistry significantly. So all in all, using neutral mechanism rates for the batch modeling, and acid mechanism rates for the transport modeling is not a too appealing approach despite it may be more rigorous.

So in conclusion, this approach is abandoned for the reasons explained. And this whole thought process is stressed because it could look somewhat suspect, and therefore needs

justification. So both the batch modeling and the transport modeling will use the same rate data, namely acid region rate data.

3.3 Thermodynamic data and mineral compositions

3.3.1 Frio thermodynamics

In this section the kinet rate data for every mineral used for simulation is evaluated.

In the acid region quartz is independent of pH and can be equated with the rates for the neutral region for the same temperatures and pressures (Palandri and Kharaka 2004). These values are taken from (Palandri and Kharaka 2004).

The mineral composition for Frio contains na-rich smecite, so a member of this family is introduced in the model in absence of a "smectite" phase in the PHREEQC database. The member introduced is na-montmorillonite. In lack of a rate constant for this particular species, the montmorillonite rate data is chosen from (Palandri and Kharaka 2004). This is not specifically a na-montmorillonite, but probably as close as one gets searching the literature.

For illite there is no kinetic rates listed in (Palandri and Kharaka 2004), so the same approach is chosen as in (Xu et al 2005), which is to set the rate to another clay member, namely kaolinite.

The kinetics of calcite is quite rapid (Xu et al 2005), so also here it is adopted the approach of (Xu et al 2005), which is to assume that calcite always is in equilibrium with the brine.

In the mineral composition source paper, (Xu et al 2005), there is made an assumption that all the plagioclase is present as oligoclase. This mineral is not present in any of the PHREEQC databases. Also it is mentioned in the same study that there is an average content of anorthite equal to 20%. Therefore it is assumed in the present study that the plagioclase is present as the endmembers anorthite and albite, with relative amounts 20% and 80%, respectively. A plausibility argument for this kind of assumption may be required, and is done by pointing to other studies in the field of reactive transport modeling where the reported plagioclase is assumed to be in the form of the mentioned plagioclase endmembers. These papers are (Iglesias et al 2009; Gaus et al 2005).

Further, hematite and k-feldspar rates are found in (Palandri and Kharaka 2004).

The resulting thermodynamic data and also the mineral surface areas are presented below. A quick note on the terms used up until now in this section. When rate data are said to be chosen from a paper, this includes all of the variables present in the following table 3.1,

except for mineral surface areas. The surface areas are all be taken from (Xu et al 2005) for Frio and (Audigane et al 2006) for Utsira. Now one should note both here and for the similar Utsira topic that implementing the data from the table below into a simulation will be very simulation specific. The log Ks are presented here just for the minerals that will potentially use them. Exactly what minerals are primary and secondary in which simulations will be clarified.

Table 3.1: Frio thermodynamic data

Mineral	Ea [Kilojoule]	Log K_{25}[log mol/m^2s]	n (Reaction order)	A [cm^2/g]
Quartz	90,9	-13,4	0	9,8
Kaolinite	65,9	-11,31	0,777	151,6
Calcite		Equilibrium		
Illite	65,9	-11,31	0,37	151,6
Anorthite	16,6	-3,5	1,411	10
K-feldspar	51,7	-10,06	0,5	9,8
Na-montmorillonite	48	-12,71	0,22	151,6
Clinochlore14A	88	-11,11	0,5	9,8
Hematite	66,2	-9,39	1	12,9
Albite low	65	-10,16	0,457	9,8
Anhydrite		Equilibrium		
Magnesite		Equilibrium		
Siderite		Equilibrium		
Pyrite		Equilibrium		
Ankerite		Equilibrium		
Dawsonite		Equilibrium		
Alunite		Equilibrium		

3.3.2 Frio mineral compositions

In this section the mineral compositions of Frio sandstone and shale is discussed in terms of how It has been implemented. The mineral composition is taken from the source study (Xu et al 2005).

A remark should be noted on the determination of the compositions reported in the source paper. (Xu et al 2005) reports that the actual determined composition of the sandstone is 56% quartz, 28% feldspar and 16% lithic fragments. Here 30% of the feldspar is K-feldspar and the rest is plagioclase with 20% anorthite content. The composition of the lithic

fragments is educated guesswork performed by the authors. The amount of clay, iron oxides and calcite was arbitrarily assigned in their study. For intimate details on this topic the paper can be looked up.

Another remark should be made on the presence of kerogen in the present study. Kerogen is treated only as a volume occupying and unreactive species. The reason for keeping this species unreactive is because of the complexity it would be to bring it into the model. For the advanced reader there is a small discussion on the implementation of (reactive) kerogen found in the source paper for the compositions, (Xu et al 2005].

Further, the authors used a 1:1 combination of the chlorite end member clinochlore, and daphnite. Daphnite is a magnesium variation of chamosite, another end member of chlorite. The daphnite mineral data are not included in any of the PHREEQC databases, and no rate data are within immediate reach. The assumption that all of the chlorite is present as clinochlore-14A is therefore made. On the bright side the clays have slow dissolution rates so it's reasonable to assume their compositions don't mean a whole lot to the end result (Gaus et al 2005).

The authors of (Xu et al 2005) reports that a more representative way of treating e.g. the chloride group could be made in using a sold solution instead of using a combination of end members. However, the present study doesn't improve on that matter, using end members both in the case of chlorite and plagioclase.

Below is presented the composition of the Frio reservoir, Frio shale, and also an 80/20 compromise (by volume) of shale and sandstone. This last composition will make up the sediment in Frio transport calculations, a low perm layer. It is chosen to look at this composition as opposed to 100% shale so that it would be a somewhat more "moderate" heterogeneity.

Table 1.2: Frio mineral compositions

Mineral	Chemical Composition	Vol % of medium		
		Sandstone	Shale	80/20
Quartz	SiO_2	40,6	17,3	21,96
Kaolinite	$Al_2Si_2O_5(OH)_4$	1,41	3,95	3,442
Calcite	$CaCO_3$	1,35	9,81	8,118
Illite	$K_{0.6}M_{0.25}Al_{1.8}(Al_{0.5}Si_{3.5}O_{10})$	0,7	25,33	20,404
Kerogen	Unreactive	0	1,77	1,416
Anorthite	$CaAl_2Si_2O_8$	2,772	0,95	1,3144
Albite-low	$NaAlSi_3O_8$	11,088	3,8	5,2576
K-feldspar	$KAlSi_3O_8$	5,74	4,27	4,564
Na-montmorillonite	$Na_{0.33}Mg_{0.33}Al_{1.67}Si_4O_{10}(OH)_2$	2,8	20,7	17,12
Clinochlore14A	$Mg_5Al_2Si_3O_{10}(OH)_8$	3,19	2,12	2,334
Hematite	Fe_2O_3	0,35	0	0,07
Porosity		30	10	14
Secondary				
Anhydrite	$CaSO_4$			
Magnesite	$MgCO_3$			
Siderite	$FeCO_3$			
Pyrite	FeS_2			
Ankerite	$CaMg_{0.3}Fe_{0.7}(CO_3)_2$			
Dawsonite	$NaAlCO_3(OH)_2$			
Alunite	$KAl_3(OH)_6(SO_4)_2$			

3.3.3 Utsira thermodynamic data and mineral composition

This section will be a discussion on both the mineral compostion and the kinetic rate data introduced. This is in contrast to the Frio discussion where this was in two separate sections. The data for Utsira requires a smaller discussion, so therefore it is kept in one section only.

The reported composition of the sandstone is measured at a depth of 1085 to 1086 meters (Audigane et al 2006), while the shale composition is taken as described by (Gaus et al 2005) who studied the caprock of Utsira, namely Nordland.

Calcite reacts very fast, so just as for Frio it is set to always be in equilibrium with the brine.

Quartz is introduced into the model, even though the source study (Audigane et al 2006) use chalcedony. Quartz is the mineral reported where the composition originates, namely (Pearse et al 1999), so that's the reason it was chosen instead of chalchedony.

K-feldspar and kaolinite rates are introduced in the same way as for Frio.

For the reported chlorite, the endmember clinochlore(14A) is used, in the same way as for Frio.

(Audigane et al 2006) introduces all the plagioclase as albite (low), and the mica/illite as muscovite, so this approach is followed in the present study. The rates are taken from (Palandri and Kharaka 2004).

For the rest of the minerals found to exist at this site, pyrite, ilmenite, apatite, zeolite and Ti xxides, are chosen by (Audigane et al 2006) to be ignored, i.e. not to be introduced into the model. It can only be assumed that this decision is made due to the low content, the biggest are only a few parts per thousand by volume. The authors seem to have attributed the tiny missing volume to quartz. The same approach is followed in the present study.

For siderite the rates are from (Palandri and Kharaka 2004).

(Audigane et al 2006) have performed an analysis of what minerals are commonly observed to precipitate under the relevant conditions, and by this decided on the secondary minerals.

The secondary minerals are dawsonite, magnesite, dolomite, kaolinite and siderite for the sandstone part, and for the shale part dawsonite, magnesite and dolomite.

Thermodynamic data are presented below in figure 3.3.

Table 3.3: Utsira thermodynamic data

Mineral	Ea [Kilojoule]	Log K_{25}[log mol/m^2s]	n (Reaction order)	A [cm^2/g]
Albite low	65	-10,16	0,457	9,8
Calcite		Equilibrium		
Quartz	90,9	-13,40	0	9,8
Chlorite	88	-11,11	0,5	9,8
Muscovite	22	-11,85	0,37	151,6
K-feldspar	51,7	-10,06	0,5	9,8
Kaolinite	65,9	-11,31	0,777	151,6
Siderite	62,76	-8,90	0,822	9,8
Dolomite		Equilibrium		
Magnesite		Equilibrium		
Dawsonite		Equilibrium		

And the composition is found in table 3.4.

Table 3.4: Utsira mineral compositions

Mineral	Chemical Composition	Vol % of medium		
		Sandstone	Shale	80/20
Albite low	$NaAlSi_3O_8$	1,74	11,847	9,8256
Calcite	$CaCO_3$	3,886	0,8975	1,4952
Quartz	SiO_2	44,602	29,9765	32,9016
Chlorite14A	$Mg_5Al_2Si_3O_{10}(OH)_8$	0,745	3,949	3,31
Muscovite	$KAl_3Si_3O_{10}(OH)_2$	3,016	22,5273	18,625
K-feldspar	$KAlSi_3O_8$	4,002	2,0643	2,4518
Kaolinite	$Al_2Si_2O_5(OH)_4$	0,0	17,5013	14,001
Siderite	$FeCO_3$	0,0	0,9873	0,7898
Porosity		0,42	0,1025	0,166
Secondary				
Dolomite	$CaMg(CO_3)_2$			
Magnesite	$MgCO_3$			
Dawsonite	$NaAlCO_3(OH)_2$			

3.4 Simulation data: Temperature, CO_2 fugacities and diffusivity

For the Utsira site this value is simply taken to be $f = 55\ atm$ according to (Gaus et al 2005).

For the Frio site however, the use of correlations as given in section 2.4.5 is required.

In the following a temperature of $T = 37°C$ is assumed for Frio. This is not the true value, but this value is chosen so that the results may somehow be comparable to the Utsira formation, where the temperature is exactly $37°C$ (Audigane et al 2006). This temperature is consistently used in the present study for any other temperature dependent quantity of both Frio and Utsira. The pressure in the Frio formation is 198,37 atm (Xu et al 2005).

From figure 2.3 a fugacity coefficient of $\phi = 0.32$ is found. Therefore the fugacity is

$$f = \phi * P = 0.32 * 198{,}37atm = 63{,}48atm$$

So a fugacity of 63,48 atm is used for the Frio gas phase simulations, and the mentioned 55 atm for Utsira.

For both sites the diffusivity is $10^{-9} m^2/s$ (Audigane et al 2006; Xu et al 2005)

3.5 Heterogeneity Scenario

The scenario that will be looked upon in the present study is discussed in this section.

The scenario studied is the effect of carbonated brine in contact with low permeable layers. The composition of these low permeable layers is created from a weighted sum of the volume fractions of sandstone and shale layers at each site. The extreme case is 100% shale, so a slightly more moderate composition is considered, namely a composition of 80% shale and 20% sandstone.

Figure 3.1 illustrates what has been done.

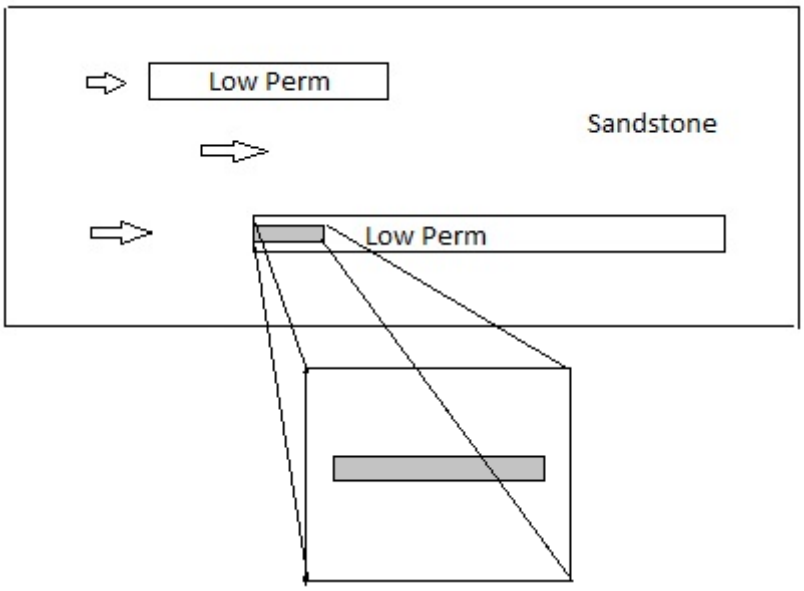

Figure 3.1: Low pereability layer as hetereogenieity scenario

As is visible in the figure, only a small part of the low perm layer is looked upon. This will be 10cm in both Frio and Utsira.

3.6 Carbonation of brine

In all of the simulations it is used a carbonated brine which is exposed to some reservoir heterogeneity and its pore water by mass transport. The carbonated brine, and the process of creating it has a few sides to it.

There are two ways of modeling the carbonation of the brine. Either with what is called an open system, or a closed system (Soong 2003). Both methods are based on imposing a high pressure CO_2 gas phase which will react with the brine. In a closed system a sparse amount of moles are awarded the gas phase, while in an open system an arbitrary amount of moles is defined. A closed system with an amount of CO_2 that is much larger than the amount

consumed by dissolution into the solution is in effect an open system. In this way only the open system will possibly be in equilibrium with a CO_2 phase at the specified pressure.

Further, since there could be injected a large amount of supercritical gaseous CO_2 into a storage reservoir, one can assume that there can be regions where it theoretically can be in equilibrium with the brine. This could especially be true close to the injector where the large amount of CO_2 flows.

So this was a question asking whether there possibly may exist equilibrium between the brine and the gaseous CO_2 phase somewhere in the reservoir. So if this "open system" assumption is made, one can proceed to the next.

The next question is a matter of both how fast and how long the carbonation process should be assumed to take place. Is it reasonable to assume that the CO_2 should instantly come to equilibrium with the brine alone as if the sediment were unreactive, or should it come to equilibrium with the both the brine and the sediment system together. These are the two end member cases for what concerns equilibrium, and it's unclear which the better assumption is.

If one were to compromise on these two options there seems to be endless paths. An elaboration of just a few of these might be interesting. For example if one firstly assumes the CO_2 gas phase to always be in equilibrium with just the brine alone, then a few cases are possible.

One could run a batch simulation for any chosen amount of time where the sediments are considered reactive. That is, from time zero and until a total equilibrium between the CO_2 gas– brine – sediment system occurs, call this t_{eq}, there will be possible to run this simulation for an arbitrary amount of time as long as the time t is $0 < t < t_{eq}$. And every different choise of time length will show slightly different brine as result.

Or one could let the CO_2 gas phase instantly come to equilibrium with the brine alone keeping the sediments unreactive, then decouple the CO_2 gas phase and let the resulting brine react with the sediment, either to equilibrium or for any amount of time $0 < t < t_{eq}$.

Or one could let the whole CO_2 gas phase – brine – sediment system be reactive, then let it come to equilibrium before one detach the CO_2 gas phase and further let the brine react with sediment alone for any chosen amount of time. Here the last step can be performed with either the sediment used in the first step, or a new "untouched" sediment batch which is more representative of the general reservoir composition. This will be applicable to many of the other possible scenarios as well.

These steps mentioned where one at some point decouples the CO_2 gas phase might be interpreted as brine that once was exposed to excessive amounts of CO_2 and e.g. has being subject to some kind of mass transport within the reservoir where CO_2 is sparser. This

touches on the assumption mentioned at the start of this topic on whether one should assume an open (excessive CO_2) or closed (sparse CO_2) system.

Further, leaving the assumption that CO_2 gas phase are always assumed to be in equilibrium with the brine, one could incorporate rate equations that calculates the amount CO_2 dissolved at any time step.

The list of options goes on and on, but this should serve as a plausibility argument that there is no solution to this that can be perfect.

The approach chosen in the present study is to first use one type of carbonated brine to obtain results both for Frio and for Utsira, and then to run an additional Frio simulation with another type of carbonated brine. This last simulation here is performed as an attempt to support some of the discussion and conclusions that are drawn from the first results. The carbonated brine for the first main results will be called type 1 brine/solution, whereas the brine used in the additional simulation on Frio is called a type 2 brine/solution.

So the type 1 brine is going to be an endpoint case. It is assumed an instant equilibrium between the CO_2 gas phase and the sandstone pore water alone. In other words this means instant carbonation of the pore water while the sediment is kept unreactive.

The type 2 brine will be sandstone pore water that is allowed to react with both a high pressure CO_2 gas phase and the sediment for an arbitrary chosen amount of time equal to 16 years.

As a finish to this section there should also be a justification of using carbonated sandstone pore water for transport into the heterogeneities, as opposed to e.g. a carbonated version of the heterogeneity pore water. One can see from figure 3.1 that the scenarios studied are at the boundaries of the heterogeneities. So the brine that is carbonated is really the one outside of the heterogeneities, namely the one found in the sandstone sediment. The scenario of interest is the one where heterogeneity has not yet been, but is about to be affected by the injected CO_2. This fits exclusively with the scenario where one carbonates the sandstone brine and not the heterogeneity brine. Therefore this will be the approach chosen in the following study.

4 RESULTS WITH DISCUSSION

In the following sections the results of both batch modeling and transport simulations are presented and discussed. In the first four sections, 4.1.1 to 4.1.4, there will (among other things) be created and used type 1 infilling solutions, and in the last two sections, 4.1.5 to 4.1.6, type 2 infilling solutions are used. This is important to note since these last two Frio section results are made as a verification of some assertions posed in the first Frio and Utsira sections. Namely there will be checked whether changing to a type 2 infilling solution may have any special effects on the results discovered in the simulations where type 1 infilling solutions were used. All of this is further explained in the following sections.

4.1.1 Frio batch modeling

So batch modeling is the part performed to create brines for further use in the transport modeling.

First one creates brine equilibrated with Frio sandstone, which is then carbonated by a high pressure CO_2 phase. This is the infilling solution.

Also one creates a brine that is in equilibrium with a heterogeneity that will be studied. This will act as the initially pore water present in this heterogeneity.

The simulation input data is not going to be perfectly identical to the ones used in the source study by (Xu et al 2005). This means that the brines that were used by (Xu et al 2005) will not be in perfect equilibrium with the system defined here. This is because there is used slightly different thermodynamic – and other simulation data here. So what is done is to use the brine composition from (Xu et al 2005) as a starting point, and further equilibrate it to the data and system in the present study. So in summary the brine is treated as follows

Sandstone brine by (Xu et al 2005) → Equilibrated with the present data → Carbonated by CO_2 gas

So the start-out composition from (Xu et al 2005) can be seen from the table below

Table 4.1: Start-out sandstone pore water composition from (Xu et al)

Element	Molality
Al	2,66e-8
C	4,32e-2
Ca	3,23e-3
Cl	1,00
Fe	2,42e-5
K	7,52e-3
Mg	1,53e-7
Na	9,90e-1
S	1,32e-9
Si	7,26e-4
pH	7,34

This is further equilibrated as can be seen in figure x below.

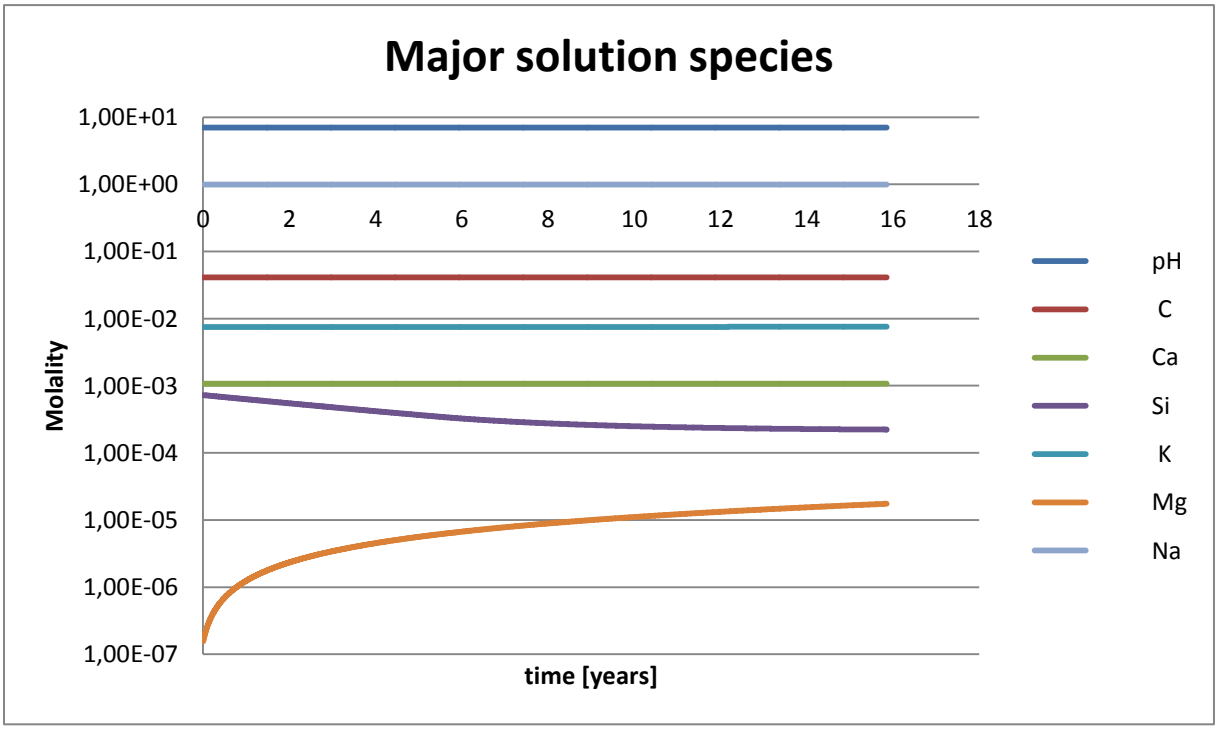

Figure 4.1: Sandstone pore water from (Xu et al) equilibrated with the sandstone sediment in the present study.

Only major species are presented in this plot. One should note here that this doesn't give the whole picture as the initial concentrations wasn't included, only step one and further is included. So since e.g. calcite is an equilibrium reactant (as described in the background section), its relatively large change in concentration that happened instantly isn't possible to see here. This will be true in all of the batch modeling results to come. As, as one can see,

the equilibration process seems to be adequate after 16 years. The carbonation process of this resulting solution is an instant process, and is shown in the table below.

Table 4.2: Frio carbonated sandstone pore water (infilling solution type 1)

Element	Molality
Al	2,07e-9
C	1,311
Ca	1,071e-3
Ca^{+2}	9,632e-4
Cl	1,00
Fe	2,954e-15
K	7,544e-3
Mg	1,746e-5
Na	9,899e-1
S	1,32e-9
Si	2,221e-4
pe	-0,587
pH	4,437

The difference in carbon content is apparent when comparing the plot 4.1 and the table 4.2. The carbonation process has increased the carbon content roughly by a factor of 20.

So what remains now is the initial pore water in the heterogeneity. The start-out solution in this case is a 80/20 mixture (by molality) of shale pore water and sandstone pore water, respectively. These pore water compositions are also taken from (Gaus et al 2005), and the calculated 80/20 mixture is presented in table x below.

Table 4.3: 80/20 Mix of shale porewater and sandstone porewater from (xu et al)

Element	Molality
Al	4,86e-8
C	7,45e-1
Ca	5,32e-2
Cl	1,00
Fe	3,98e-4
K	1,55e-3
Mg	5,48e--7
Na	8,62e-1
S	7,78e-7
Si	6,16e-4
pH	6,81

The equilibration process is shown in figure x below

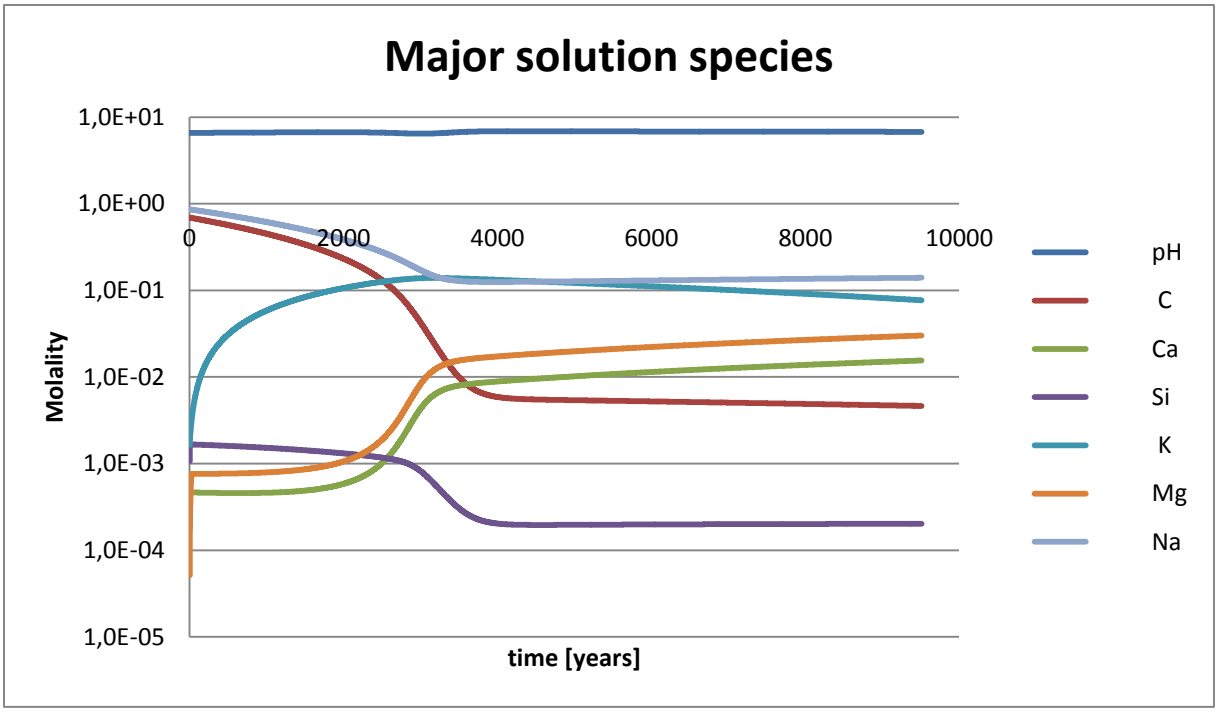

Figure 4.2: Equilibrating the 80/20 mix of shale pore water and sandstone pore water from (xu et al) with the hetereogenieity sediment.

Also here only major species are shown. The values one can see after nearly 10 000 years, together with some minor species are shown in table 4.4 below.

Table 4.4: Initial porewater for the hetereogeneity

Element	Molality
Al	8,486e-8
C	4,63e-3
Ca	1,551e-2
Ca^{+2}	1,532e-2
Cl	9,975e-1
Fe	3,217e-14
K	7,688e-2
Mg	3,010e-2
Na	1,399e-1
Si	2,018e-4
pe	-3,306
pH	6,764

4.1.2 Frio Diffusive transport

In this simulation, diffusive transport of carbonated sandstone brine is interacting with the described rock column. The total length of the column is 10 cm. More details on this are presented in the data section.

Results that are of relative importance are presented together with a grid size sensitivity simulation. This is to give an impression of the accuracy in the results since the simulation tool used may be subject to numerical dispersion. The number of grid cells used in the runs is 80 and 160 which in the following is referred to as a coarse and a fine grid, respectively. The uncertainty due to numerical dispersion generally seems to be in the order of 10^{-3}, but sometimes also in the order of 10^{-2}.

So numerical accuracy might be somewhat unsatisfying, and a drawback in some of the results. But further fining of the grid would require an inadequate amount of time to run. So this is going to be a limitation, but an identified one. The required simulation time is also a reason for the somewhat short time period studied, namely 60 days. Generally the system shows to be quite unreactive at this small timescale.

Now that some details are handled, a discussion of the results. Imposition of a high pressure CO_2 gas phase has created a low pH in the infilling solution. As is shown in table 4.2. This causes the diffusion of protons into the heterogeneity which means a general drop in pH throughout the whole length. The diffusion of protons into the heterogeneity is shown in the figure 4.3 below.

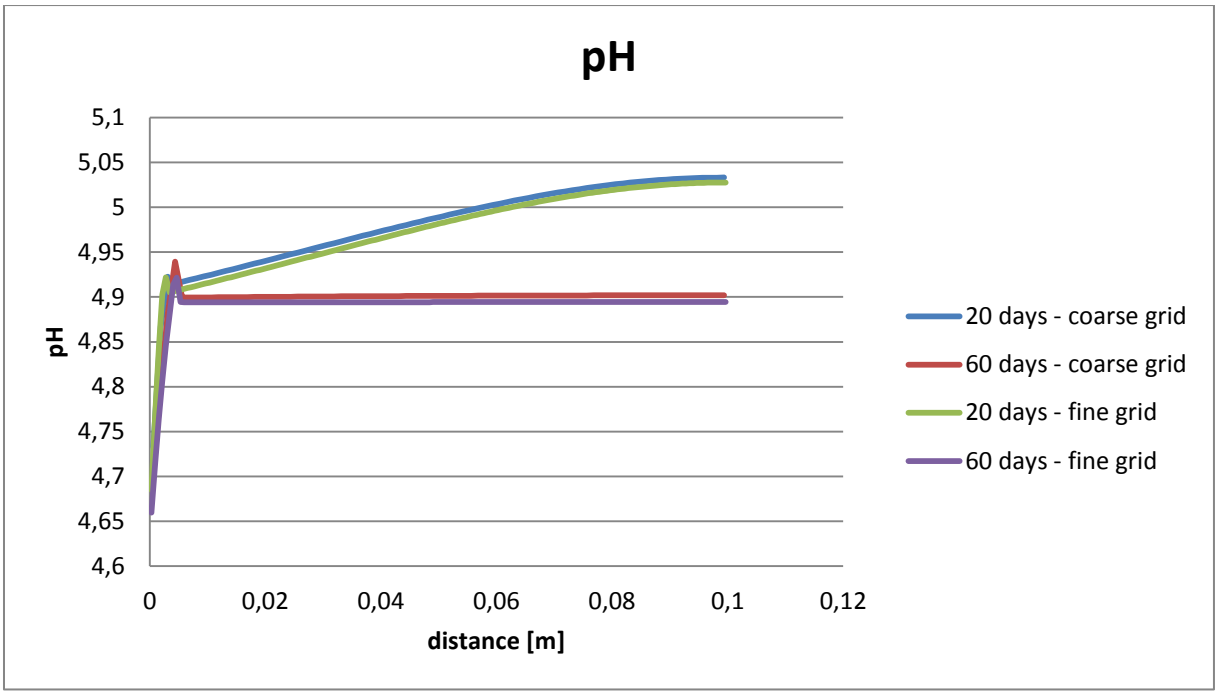

Figure 4.3: pH result shown at different times

This result is shown for 20 days and 60 days, and includes sensitivity on the grid size. It is stressed that the boundary condition is chosen as “constant”, which is described in the theory section. Also important to note is that it’s not in contact with any mineral assemblage in itself. This will make it appear somewhat as a “sink” or “pump” for some species, namely for those where the difference is big across the boundary to the heterogeneity. This is

already evident in the pH plot, where one can see a rather steep transition zone at the inlet. And it is going to be quite more evident in the following analysis of calcite dissolution.

The lowering of the pH triggers calcite dissolution. Calcite shows to be highly reactive at a very tiny distance from the inlet. The calcite content can be seen from figure 4.4 below.

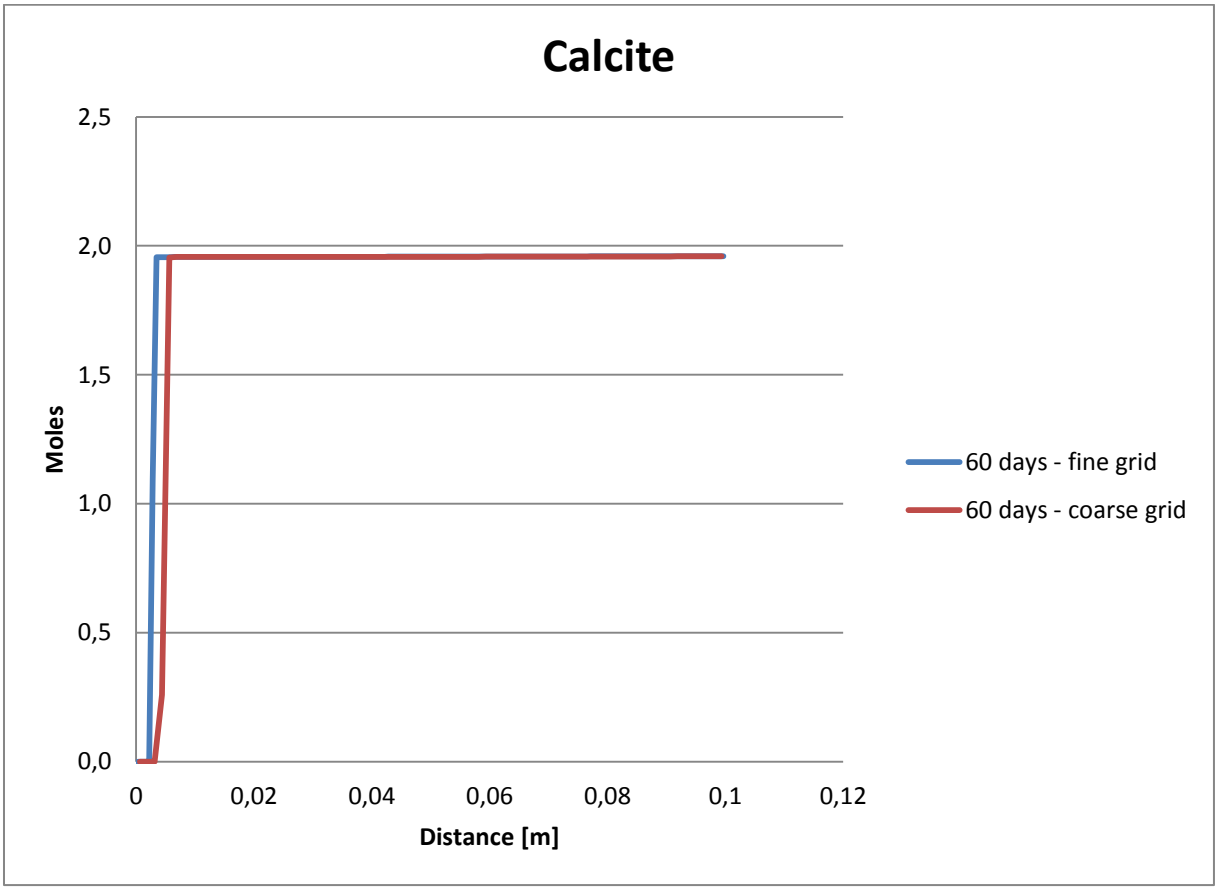

Figure 4.4: Calcite moles vs distance in the hetereogeniety

After 60 days all the calcite has been dissolved in a distance within roughly 0,4 cm from the inlet. But less than half this distance further into the column there seems to have been only minor dissolution, as is also the case throughout the rest of the length. In the fine grid run there have been used 160 grid cells. At the end of the simulation, the first seven of these cells have all their calcite dissolved, and the eighth cell is reduced to contain only a small fraction of its original content. It seems that the dissolution of calcite is completed in steps, with total dissolution in the first cell before any significant changes happen to the next one. This will be further addressed in the following. But before continuation, a note on the grid size and accuracy.

In the first few cells there seems to be quite large discrepancy due to the large calcite dissolution. Rendering this tiny first part perfectly would probably require a vast amount of

time, or a very powerful computer. Essentially, the disagreement in the results lies in exactly which one is the last cell where calcite dissolution is ultimate. This is not of any great importance.

So in the following, it is first investigated what creates this large calcite dissolution just observed to take place. Then it is shown that the importance of mass transport by diffusion on the calcite dissolution increases drastically by just small increments in distance from the inlet.

So already it is shown that the heterogeneity is served protons in abundant amounts from the infilling solution. Now carbonate has to be altered to bicarbonate or removed in other manners as a first step for calcite to dissolve. Since the pH is in the intermediate region, bicarbonate will be dominating in presence in place of carbonate, as is shown in the chemistry section 2.3.2.

It is noted that there is a higher abundance of calcium in the heterogeneity brine than in the infilling solution, so this species will be diffusing out of the heterogeneity.

So the calcite dissolution is induced by turning the carbonates into bicarbonate, as well as the calcium diffusing out of the heterogeneity. For this to be a plausible explanation, the ability of the infilling solution to remove the calcium must be quite large, and is attempted shown in the following figures.

In figure 4.5 below Ca^{2+} is shown.

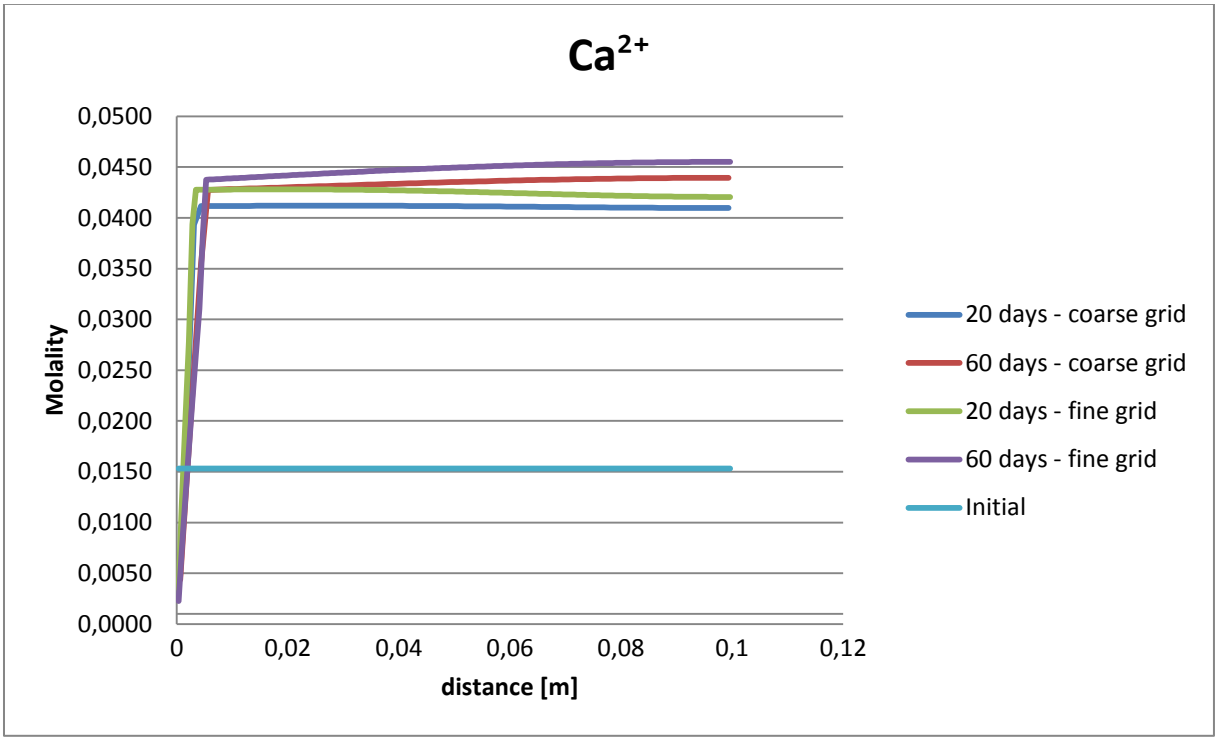

Figure 4.5: Ca^{2+} molality vs distance

The grid sensitivity is shown in the same figure. It is evident that there is very small calcium concentration in the infilling solution, draining the heterogeneity. This is especially evident in the first cells.

A zoomed graph of Ca^{2+} is presented below in figure 4.6.

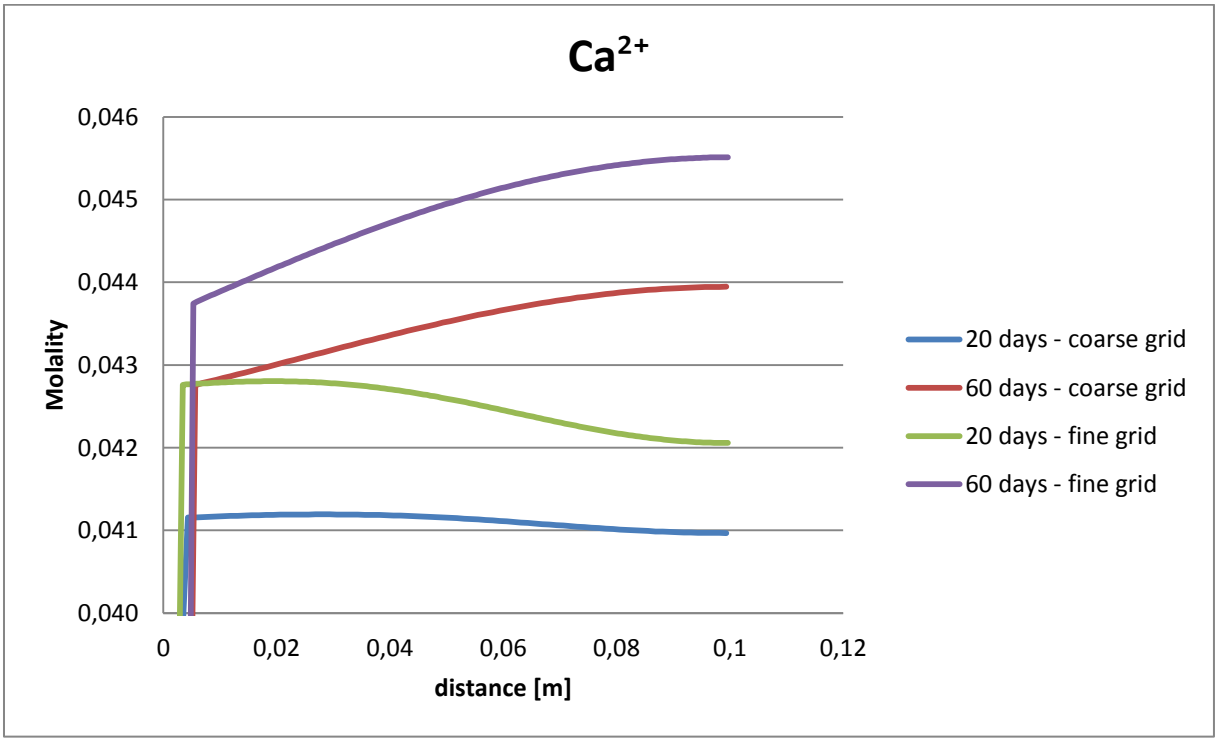

Figure 4.6: A zoomed Ca^{2+} molality vs distance

So one can first see that the error is quite small in the grid sensitivity. Also the Ca^{2+}distribution throughout the reservoir seem quite uniform, except at the inlet where the concentration is far lower. As one can see, in this region it's even a lot smaller than the initial amount.

The extent of calcium diffusing out of the heterogeneity is shown by some more simple calculations and graphics. First, for this purpose a distinction is made on the first 8 cells and the last 152 cells. This is meaningful because both the abundance of calcium and calcite is somewhat similar within these blocks. As already mentioned many times, after 60 days the first block (first 8 cells) has almost all its calcite content dissolved, whereas only a small amount is dissolved within the other block (last 152 cells).

So the figures below show how many moles of Ca^{2+} that in total have been in "touch" with the brine. This is the initial amount plus the amount produced through calcite dissolution. Any other effects show to be too small to be considered. The figure containing the results (figure 4.7) from the first 8 cells has to use a log scale to be meaningful since the amount dissolved is vast when compared to the remaining content.

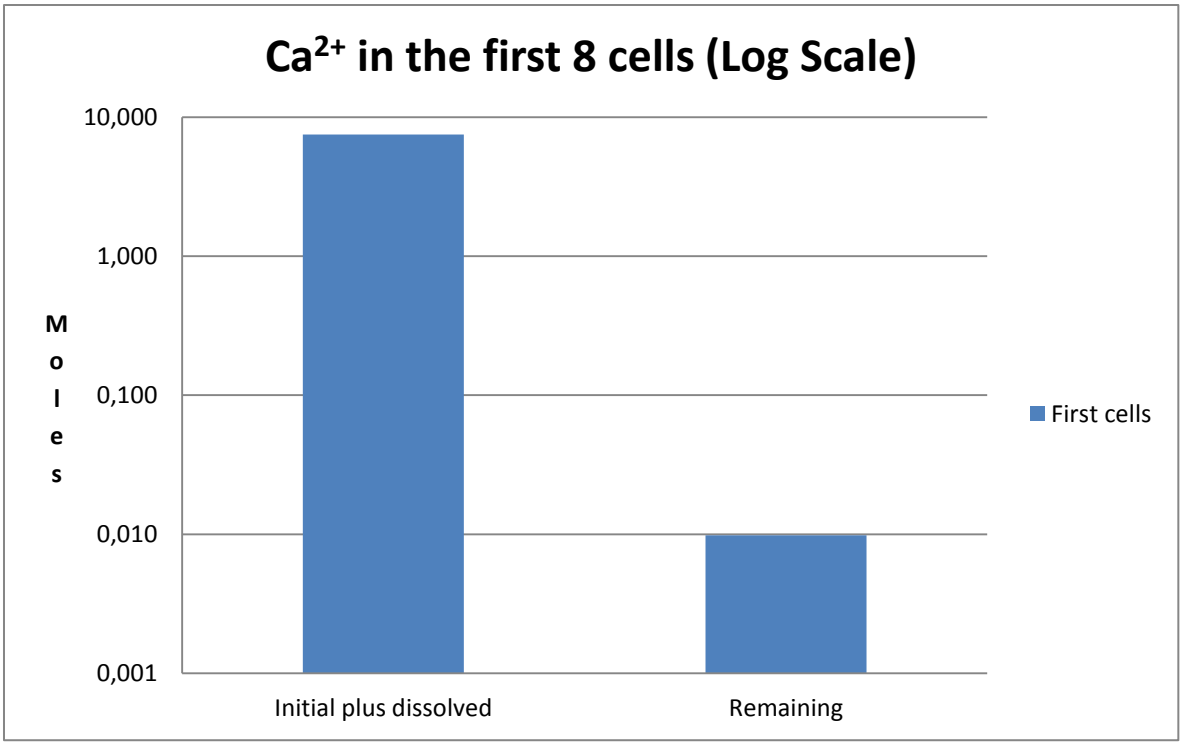

Figure 4.7: Moles of Ca^{2+} that was initially present in the first 8 cells plus the moles dissolved here, compared to the remaining moles after 60 days.

On the next figure, Figure 4,8, one can see that there has been at least a small amount of calcite dissolution in the last 153 cells. Note that now there is not a log scale on the vertical axis, as in the last figure. These cells are farther away from inlet, so only minor amount is lacking.

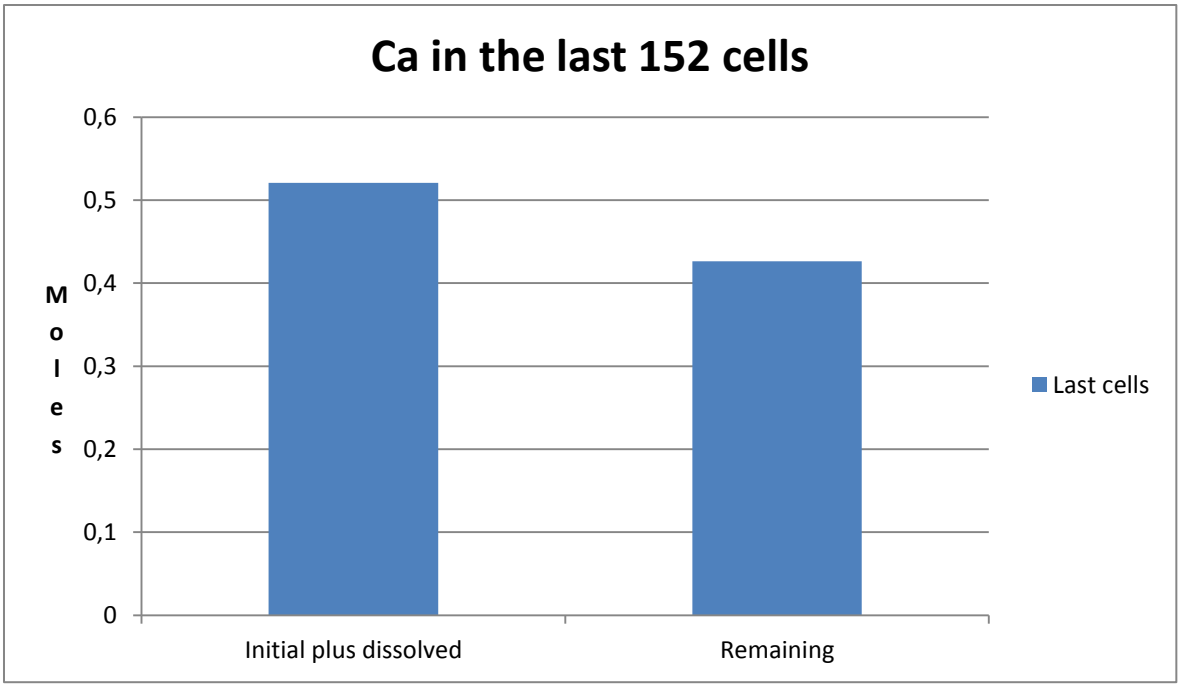

Figure 4.8: Moles of Ca^{2+} that was initially present in the last 152 cells plus the moles dissolved here, compared to the remaining moles after 60 days.

Summarizing the last two figures, the distance from the infilling solution must have played a significant role. The first cells have had their calcium content diffusing out to a very large degree, while the last ones are not too affected.

It should now be plausible that the ability to dump calcium into the infilling solution is large enough so that it together with the constant supplies of protons to alter carbonate into bicarbonate reveals the reason behind the large calcite dissolution in the first part of the column.

Now over to the last observation on this matter. It seems that even tiny increments in distance from the infilling solution contribute significantly in reducing calcite dissolution rates.

Through time it is observed that the first cell is emptied of calcite quite a lot faster than the next is emptied, and so on. In a more mathematical language, the dissolution of calcite appears to be close to ultimate/finished at distance x before significant dissolution appears in distance x+dx, and the process of dissolving the calcite at distance x+dx requires relatively more time than dissolving the calcite at distance x.

One cell difference is a very small distance, but it appears to make a significant difference after all on the dissolution rate. In figure 4.9 below the illustration shows the increasing time required to dissolve the full amount of calcite throughout the first 7 cells in the model. The resolution of this simulation is 2 days, but none of the cells are emptied of calcite exactly at

an integer multiple of 2 days. So e.g. to dissolve the calcium in cell 3 and 4 both requires at most 6 days, and at least 4 days. Also it should be remember here that this plot is only possible due to the apparent stepwise dissolution taking place, where dissolution in one cell is finished before the next. So the stopwatch for dissolving cell 7 starts the moment where cell 6 has finished.

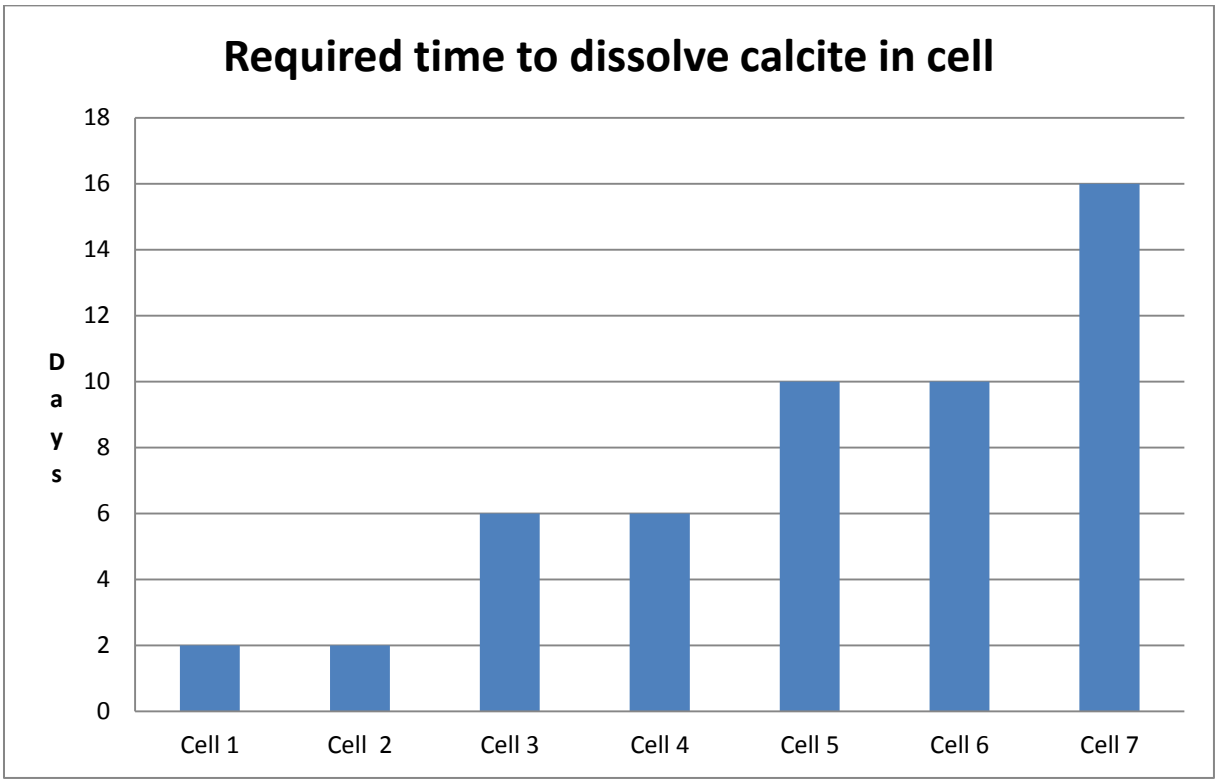

Figure 4.9: Time required to dissolve the full calcium content in cell. The time count starts when the previous cell has its content dissolved.

Since there are 160 cells, and each cell is of a length equal to one 160th of 10 cm, this should really show the importance of diffusive transport as dissolution rate limiting mechanism. Cell 1 requires 2 days to dissolve, whereas cell 7 requires 16 days, and these separated only by 0,3 cm.

Further, as mentioned in the beginning of this topic, apart from the calcite dissolution, the system is quite unreactive. The biggest reason for this is probably the small time scale studied, only 60 days. In spite of this there will soon be presented a closer look on some of the minerals. So ending the calcite study here, a look on dawsonite follows.

Change in dawsonite is showed in figure 4.10 below.

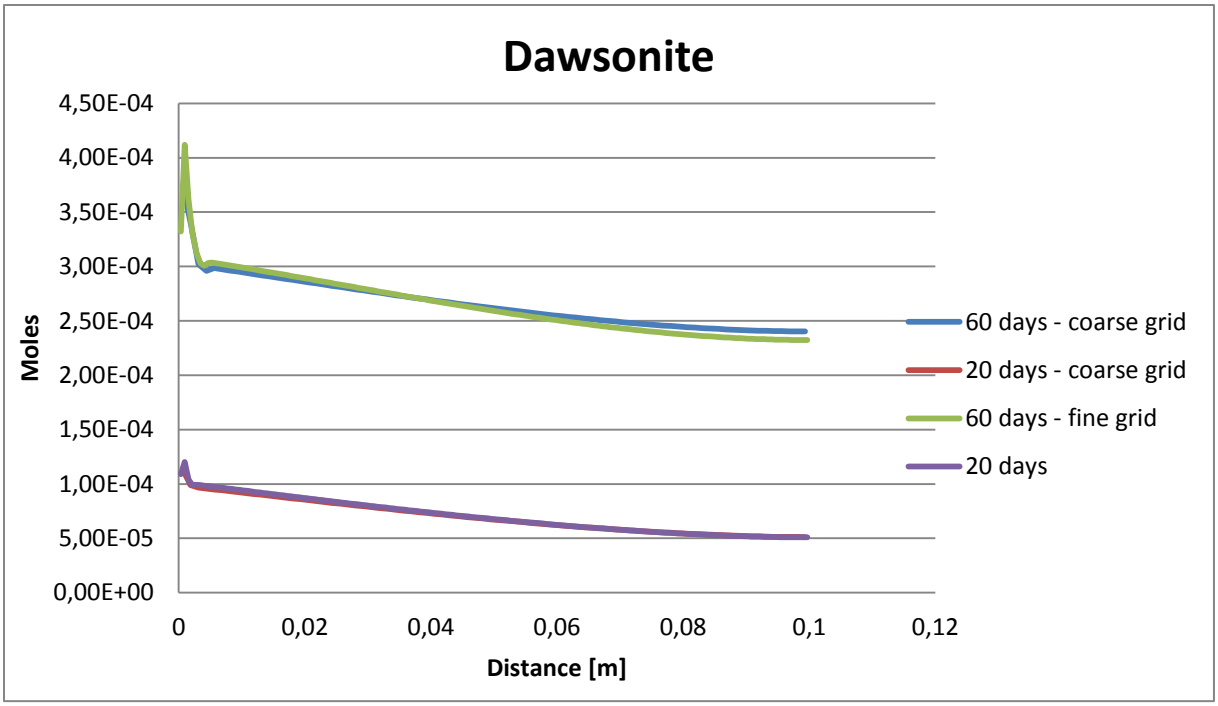

Figure 4.10: Dawsonite moles vs distance. Dawsonite was not present initially

Dawsonite is treated as a secondary mineral, so there were zero moles of this mineral present initially. Only minor amounts have precipitated at 20 days, but more than twice as much at 60 days. (Gaus et al 2005) reports the main conditions required for dawsonite precipitation to be the presence of concentrated sodic solutions together with aluminium minerals, or CO_2 and silicates rich in alkalis. This is the case here.

The grid sensitivity is fairly good in this case. The trend is decreasing amounts farther from the infilling solution, and a peak level just at the inlet. Without exception throughout the simulation, this peak always occurs in the second grid cell when 160 cells are used. It is not proposed any explanation to why this is the case.

The rest of the the result section for Frio will consist of a series of lemmas to understand this dawsonite precipitation.

First it should be mentioned that the increments in dawsonite content seems to be in the order of 10^{-6} moles per day throughout the simulation. The initial content of aluminium is rather sparse, as can be seen from table 4.4, too low to explain this dawsonite precipitation. There is however a variety of aluminium containing minerals dissolving at a similar rate as dawsonite is precipitated. These include illite, montmorillionite, anorthite, albite low and k-feldspar. The natrium constituent of dawsonite is abundant, as will be seen later. But carbonate and hydroxide is not too abundant, they vary around 10^{-6}-10^{-7} throughout the simulation. This is about the same levels as the aluminium concentrations.

So in the following there will be presented graphs that shows where the aluminium for dawsonite precipitaton is coming from. It is mentioned here, and it should be stressed that

the change in moles in the coming mineral-graphs are not meant to be accurate, so there is no grid sensitivity performed for these. The changes are in the order of 10^{-6} moles during the time period studied. Aspiring such numerical accuracy did not show to be fruitful. The uncertainty is going to be just as large as the change in moles. So since only the trend is going to be important here these runs are performed using 40 grid cells only. In between the mineral graphs will be presented some graphs showing solution species. These are included as supplements just to discuss why the minerals have dissolved in the way they have. But note here that even though the changes in minerals assemblages are too small to be presented together with accurate grid size sensitivities, the solution species will be presented with such. The changes in many of the solution species are far greater than those of the minerals, so here accurate numbers will be strived for.

So just to summarize what the rest of this section will be devoted to. The focus will be to describe what severs the aluminium supply for dawsonite precipitation. As mentioned, this will be done studying five aluminium containing minerals. Or more accurate, this will be done studying al-containing mineral which also has a dissolution rate not significantly smaller than the dawsonite precipitation rate. There are others also, but their dissolution rate was considered trivial and is therefore not included in this analysis.

So this will be the main line, but there will be a few side tracks here. These will discuss the dissolution of the minerals just mentioned in regards to the rate equation, E-1. In this equation most values are constant during the simulation, except for the reaction quotient and the proton activity. The proton activity is for simplicity taken to coincide with the pH. This is not rigorous of course but this will just be a loose discussion. For the discussion of the reaction quotient, there will be brought in some graphs of a few solution species. These are just to show whether one can see any trend in their concentration profile coinciding with increased mineral dissolution rates. If the reaction quotient is important, then a mineral should show increased dissolution rate in areas where its elements are sparse in solution. I.e. where the reaction quotient has a relatively low value. So also in this case it will be looked at concentrations instead of activities, just as for the mentioned proton activity.

Note that there will not be stated any strong positive assertions in the following section. It will merely be a loose discussion on mineral dissolution. The readers may form their own picture on this matter, but with this analysis presented here as a contribution. This is stressed just to make sure there is clarity in the ambition. Mineral dissolution / precipitation in this context are namely very complex.

K-feldspar has been dissolved, as shown in figure 4.11 below.

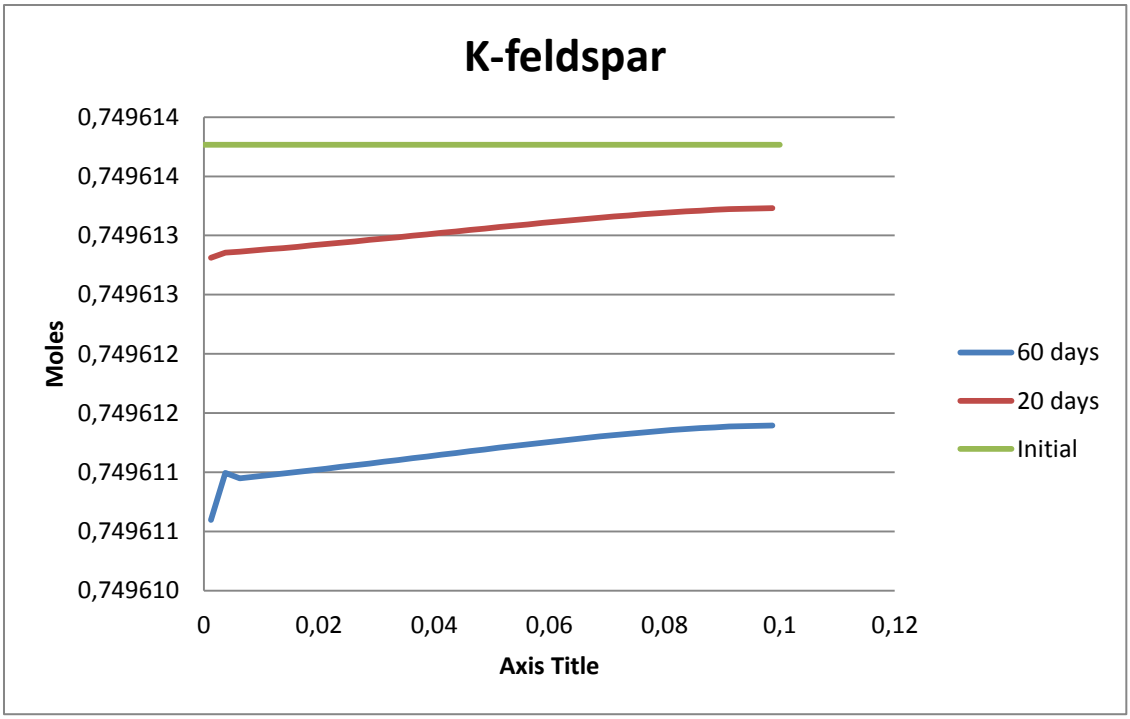

Figure 4.11: K-fedlspar moles vs distance. K-feldspar has dissolved faster towards the inlet side. This is the first of the al-supplying minerals being studied. No grid sensitivity is performed for these minerals.

The result is shown for three stages, as can be seen in the legend. The dissolution seems to be largest closer to the inlet. With time it's becoming more and more apparent that the dissolution rate has a significant jump in the first few cells. This coincides very well with the pH graph (Figure 4.3). The the first few cells has a significant decrease in pH, while an increase is shown moving through the reservoir. So considering equation E-1, the proton activity seems to be very important.

Further, it should be noted what elements make up k-feldspar, seen from equation C-13. These will be studied before the next four al-minerals is considered. This is part of the mentioned reaction quotient analysis of equation E-1. The first one is silicon, so a graph of

silicon concentration with time can be seen in figure 4.12 below.

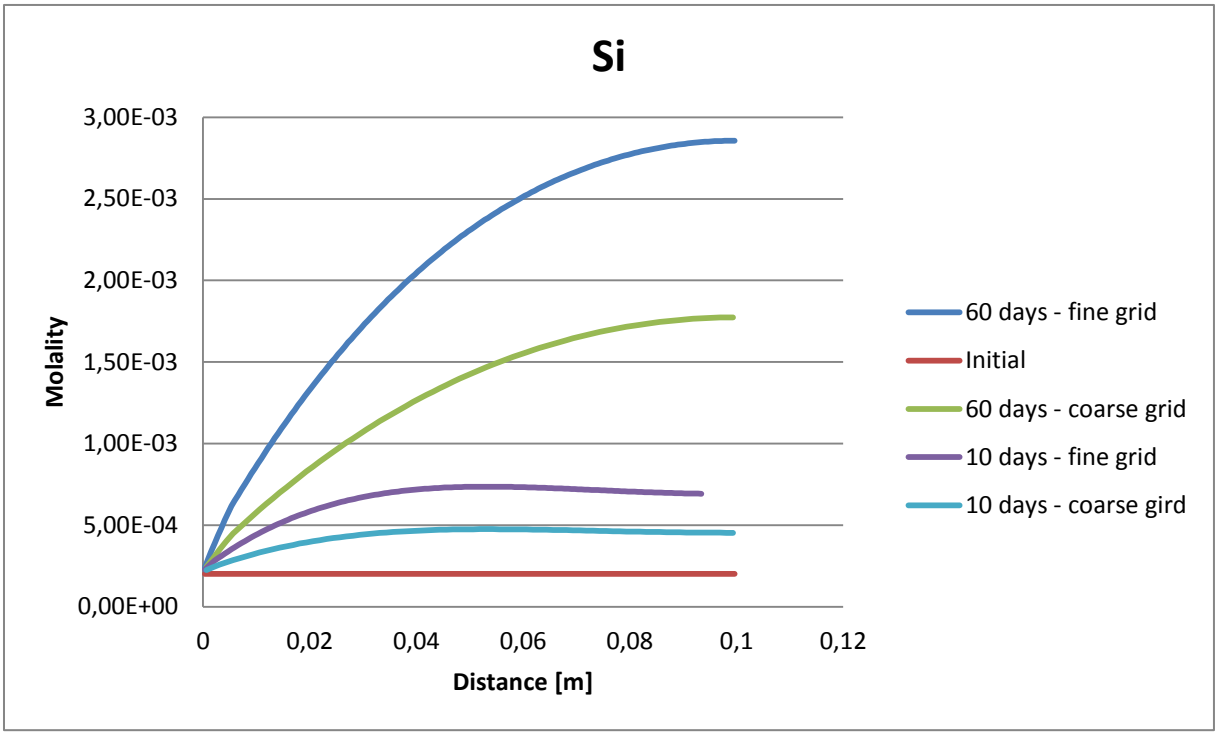

Figure 4.12: Silicon molality vs distance

The uncertainty seems to be in the order of 10^{-3}. Most of the primary minerals contain silicon, so triggering dissolution of these causes it to increase in abundance during the simulation, as can be seen in the figure. This quickly makes silicon more abundant in the heterogeneity than in the infilling solution, so this species will effectively be diffusing out of the heterogeneity. Therefore the silicon concentration tends to increase with distance from the inlet.

Further a look at potassium, the second constituent of k-feldspar. This is presented in the figure 4.13 below.

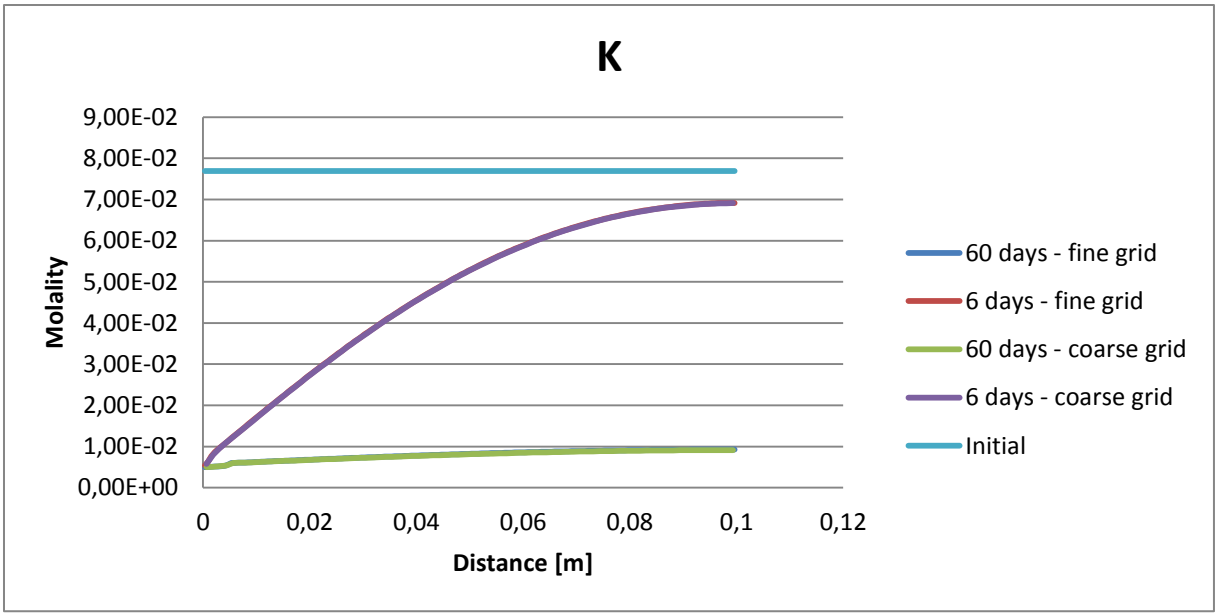

Figure 4.13: Potassium molality vs distance

There is no difference shown in the grid sensitivity, probably because the changes are relatively large. The smallest abundance is here found near the infilling solution due to diffusion, and increasing amounts farther away.

So until now it is revealed that both silicon and potassium are diffusing out of the heterogeneity, making their concentrations lowest at the inlet. So if aluminium concentration is not abnormally large here, one wouldn't be surprised finding areas closer to the inlet to have the largest k-feldspar dissolution when the reaction quotient is evaluated singlehandedly.

So an inspection of aluminium behavior follows. Aluminium is presented in the figure 4.14 below.

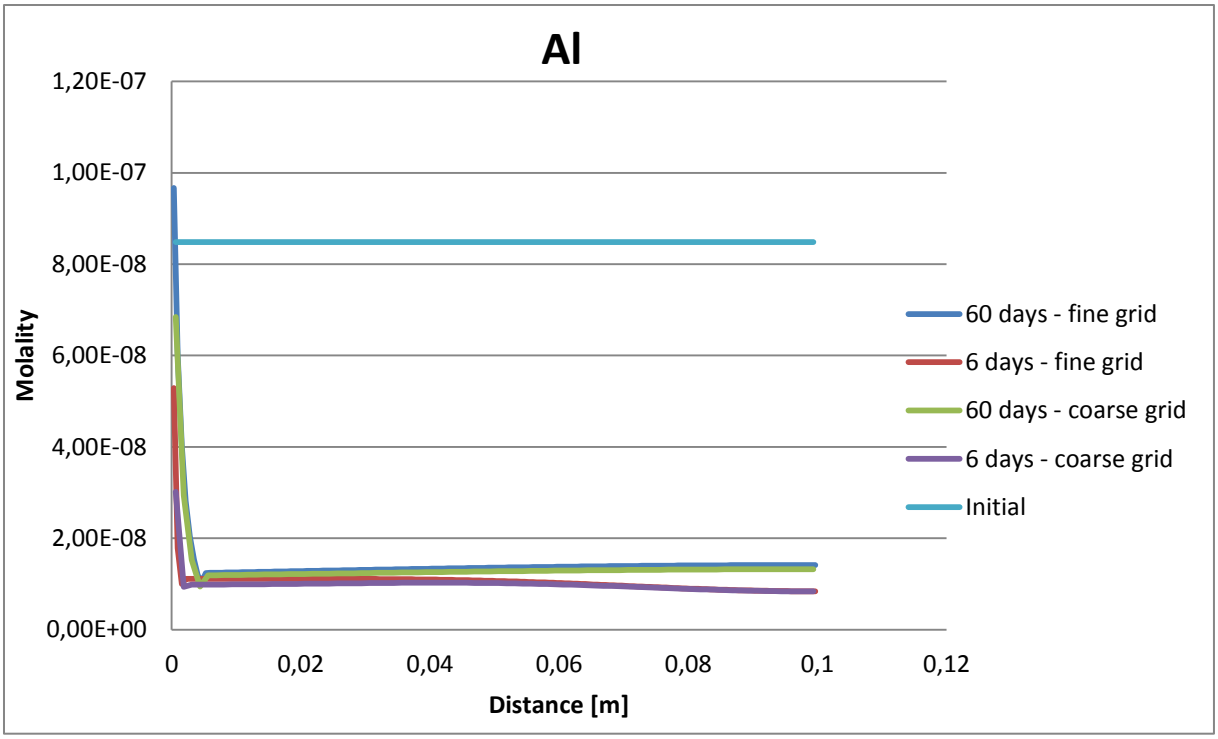

Figure 4.14: Aluminium vs distance

The grid sensitivity seems good even for the small numbers seen here. The aluminium levels drops in the entire heterogeneity from the start. But while most of the cells reach and remains at a low concentration, the abundance increases in the first few cells.

So towards the inlet end, two out of the three element constituents of k-feldspar are reduced concentrations, whereas the third mineral, aluminium, is constant through almost the entire column, but is at elevated concentrations in the first few cells only. Also k-feldspar is shown to have increased dissolution closer to the inlet. So now one could carefully suggest that despite the elevated aluminum concentration, the lowered concentrations of both silicon and potassium towards the inlet may have contributed to increasing the K-feldspar dissolution rate through the reaction quotient. This “two out of three” doesn’t seem to be a too strong correlation, so the elements of the rest of the minerals will also be studied. But this is essentially the analysis that will be applied to the rest of the al-containing minerals.

So the trend for albite low is presented in the figure below.

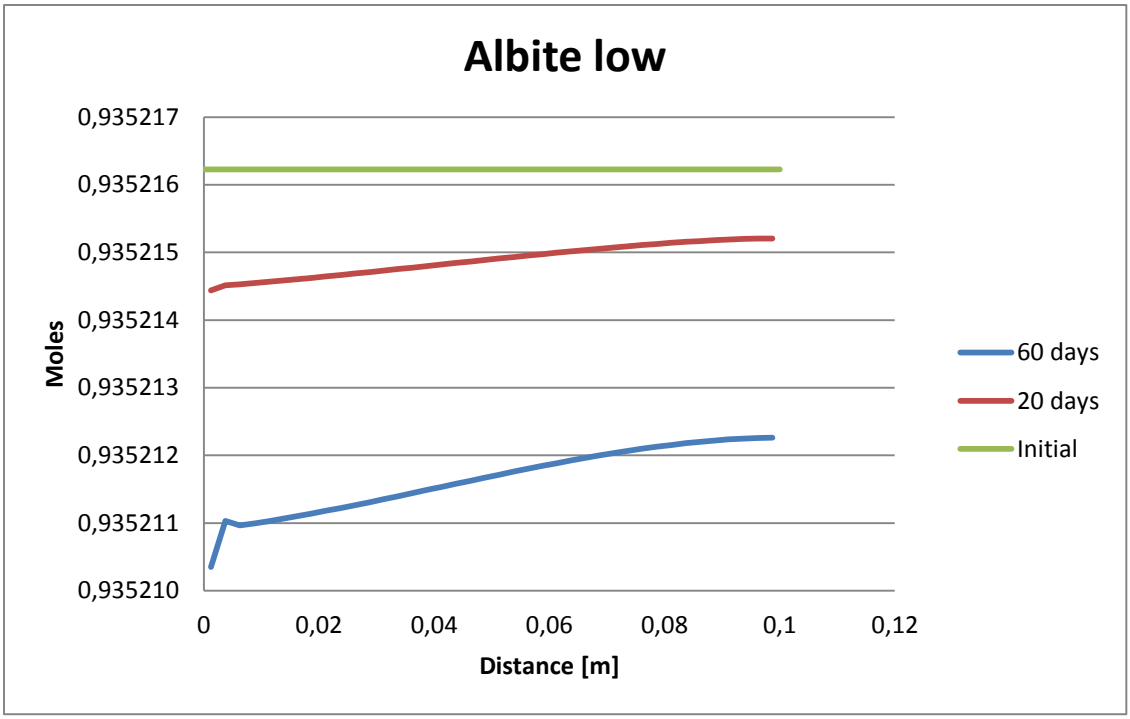

Figure 4.15: The next al-supplying mineral is albite low. There is shown moles vs distance, with no grid sensitivity.

As can be seen from the figure, albite has the same trend as k-feldspar, being dissolved faster towards the inlet, and significantly faster in the first few cells. And again one can mention that it coincides very well with the pH, or supposed proton activity.

Further the solution species from albite will be looked at, just as for k-feldspar. So the only new element here is natrium, as can be seen form equation C-11. The other elements of albite, namely silicon and potassium, were discussed in the previous section for the k-feldspar.

Na is presented in the figure 4.16 below.

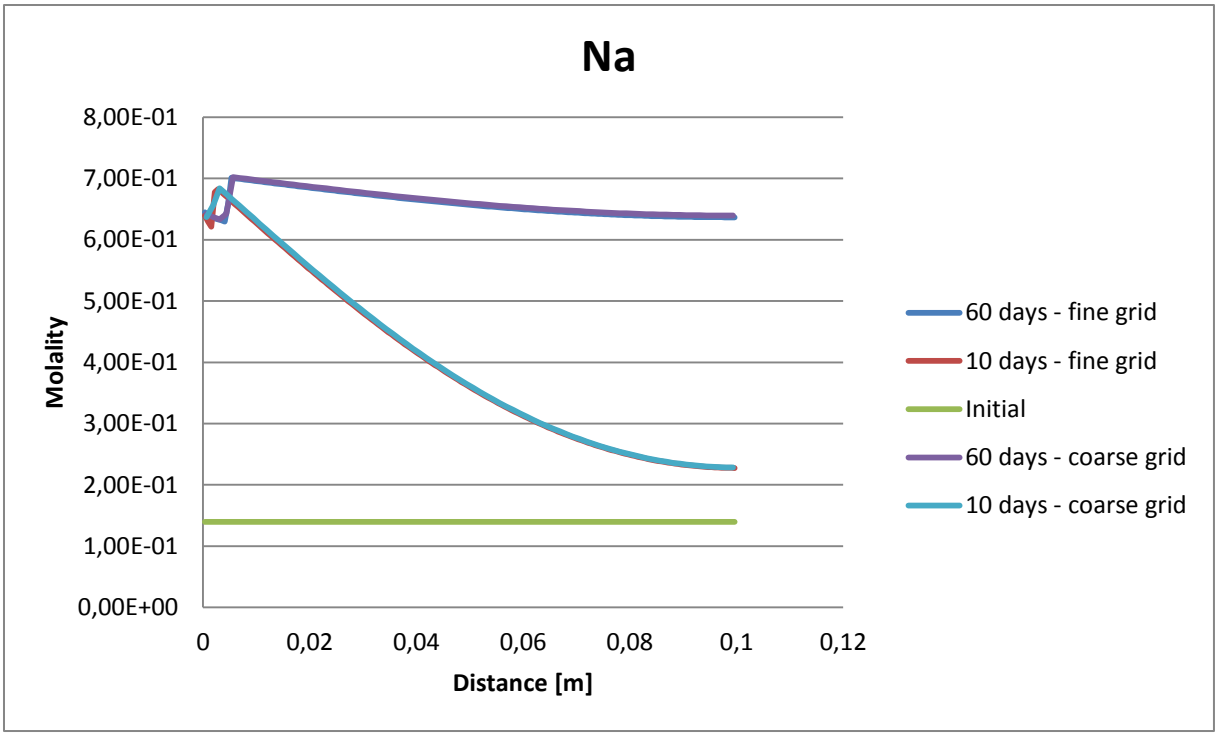

Figure 4.16: Natrium molality vs distance

The grid sensitivity is rather good, which seems to be true for all solution species with significant changes in concentration.

Further, natrium is initially in lower abundance than in the infilling solution, and does not increase beyond this during the simulation. But it does increase, as is evident from the figure above.

So natrium doesn't seem to contribute to the increased dissolution of albite towards the inlet through the reaction quotient. Actually it probably counters it to some amount since it has a higher abundance towards the inlet.

So summarized the silicon and potassium concentration may contribute via the reaction quotient, but aluminium and natrium doesn't seem to help. Natrium may even counter it having the reverse concentration profile of what is sought after here.

The next mineral will be illite, as shown in the figure 4.17 below.

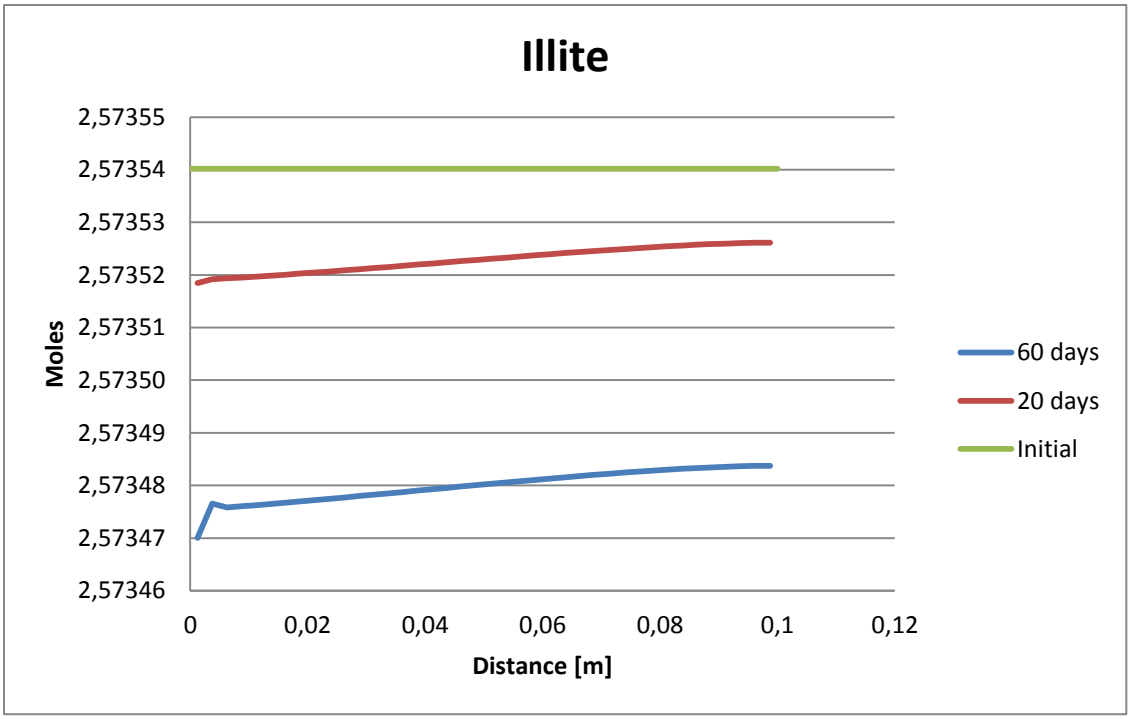

Figure 4.17: Illite moles vs distance. Illite is the next al-supplying mineral.

The same trend is found for illite as for the other minerals, dissolving faster closer to the inlet. And again the proton activity should be a good predictor for the dissolution.

For illite the elements are seen in equation C-14 to be potassium, aluminium, magnesium and silicon. The unstudied element here is magnesium. Magnesium is presented I figure 4.18 below.

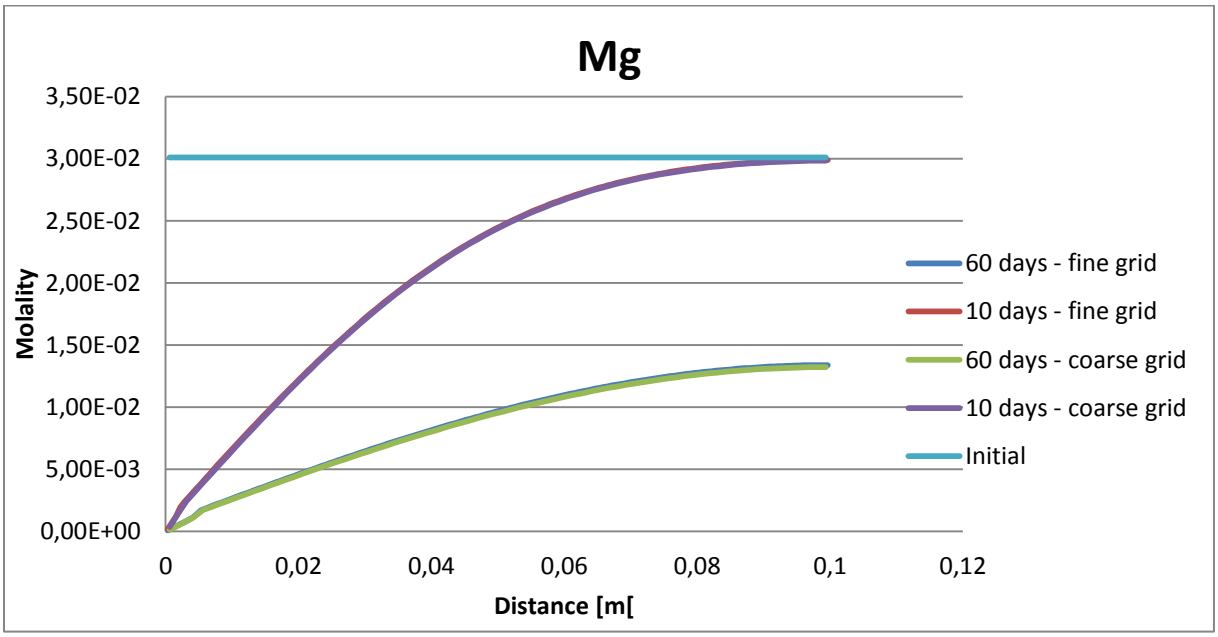

Figure 4.18: Magnesium molality vs distance

The grid sensitivity looks accurate here. Mg is far more abundant in the heterogeneity than in the infilling solution, so this is definitely going to be diffusing out, pretty visible from the figure. As usual this means a lowered concentration of magnesium towards the inlet.

So for the illite mineral, magnesium, potassium and silicon may contribute to the dissolution profile through the reaction quotient, but as already discovered, the aluminium doesn't seem to.

Anorthite is shown in the figure 4.19 below.

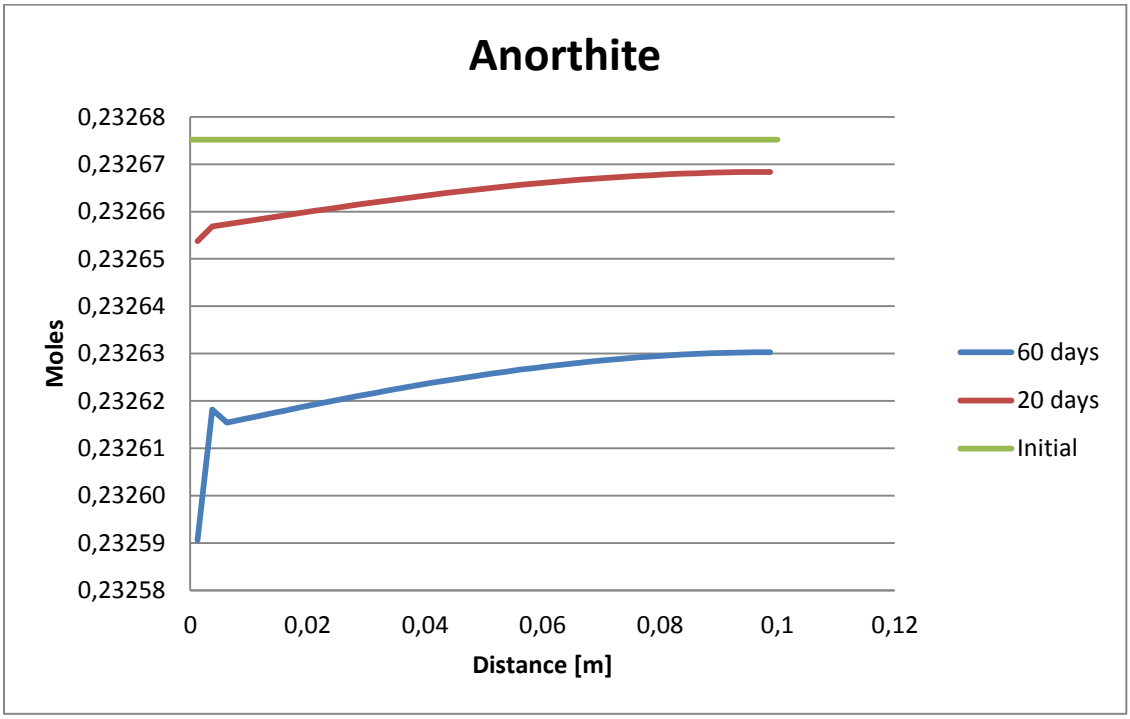

Figure 4.19: Anorthite moles vs distance. This is another al-supplying mineral.

So again the pH seems important for the dissolution rate profile. For anorthite one needs to look at calcium, silicon and aluminium, as seen in equation C-12. One already knows that calcium will be in far lower concentrations in the first few cells than the rest of the column, most of the simulation at least. This became evident in the calcite dissolution analysis.

This means that both silicon and calcium concentration profiles are consistent with the dissolution rate profile through the reaction quotient variable.

The remaining al-containing mineral is na-montmorillonite, shown in figure 4.20.

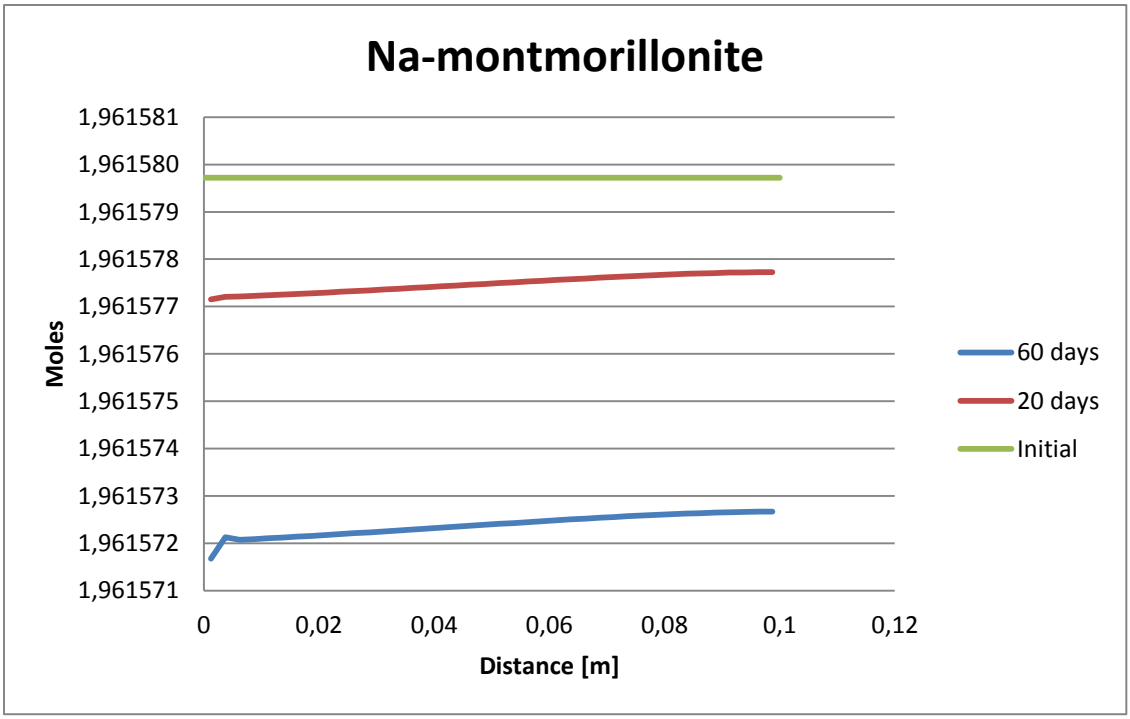

Figure 4.20: Na-montmorillonite as the last al-supplying minerals studied in this section. There is shown moles vs distance.

The pH seems significant as always on the dissolution. As for the other minerals, the trend is increased dissolution towards the inlet. The elements that are from equation C-23 shown to be relevant here are natrium, silicon and magnesium, all which have been discussed.

Silicon and magnesium have the concentration profile which is consistent with increased dissolution rate towards the inlet, while natrium has the opposite.

So in conclusion one can safely say that the pH should be tied very closely with the proton activity in equation E-1. The dissolution of every mineral is very consistent with the pH profile. The big jump in dissolution rate across the first few cells, and the constant drop off through the rest of the reservoir is nearly identical to the pH plot. So there is no doubt the pH drop is the most important contribution factor here.

When it comes to the reaction quotients, there seems to be at least some consistency. All of the minerals considered contain aluminium whose concentration profile doesn't look to be tied to mineral dissolution rates. However, apart from this aluminium, and natrium, all the other elements show a concentration decrease towards the inlet. This is consistent with a lowered reaction quotient towards this direction, which again is consistent with minerals dissolving faster in this direction. This is how it should be according to the mineral graphs presented.

At last, the dawsonite seems to be the mirror image of these dissolving al-minerals. The jump in abundance in the first few cells, and a slow decrease through the heterogeneity. It is

evident that the aluminium missing for dawsonite precipitation is coming from these minerals. And as just mentioned, at least it is clear that the incoming protons are inducing these minerals to dissolve. And maybe a weak correlation is also seen in the decreasing solution species towards the inlet, affecting the reaction quotient, which again affects the dissolution of minerals.

4.1.3 Utsira Batch Modelling

The start-out composition taken from (Audigane et al 2006) is shown in table 4.5 below. There is made no distinction between shale and sandstone pore water since only shale pore water was given in (Audigane et al 2006).

Table 4.5: Start-out sandstone pore water composition from (audigane et al)

Element	Molality
Al	0,4542e-15
C	0,1973e-1
Ca	0,3701e-3
Cl	0,5375
Fe	0,4096e-14
K	0,1553e-2
Mg	0,2576e-5
Na	0,5439
S	0,1024e-14
Si	0,1811e-3
pH	7,67

Just as explained under the Frio batch modeling topic, this solution is equilibrated with the Utsira sandstone sediment before it is carbonated with a CO_2 gas phase. The result for major solution species are presented below.

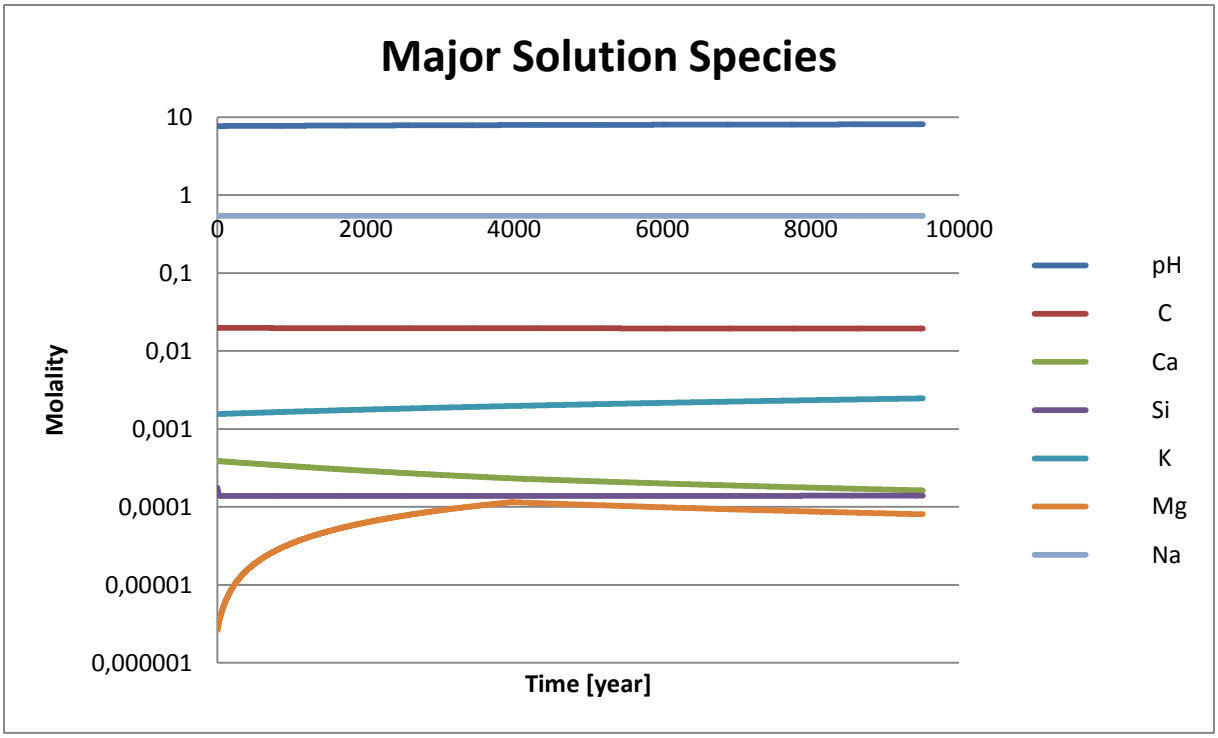

Figure 4.21: Pore water from (Audigane et al) equilibration process with the present sandstone sediment

As one can see from the figure the process was run for almost 10 000 years, and the equilibrium seems to be satisfying. So again the carbonation of this resulting brine is an instant process, and the result is shown in the table 4.6 below.

Table 4.6: Carbonated sandstone pore water (infilling solution type 1)

Element	Molality
Al	6,049e-8
C	1,181
Ca	1,628e-4
Cl	5,375e-1
Ca^{2+}	1,525e-4
K	2,467e-3
Mg	8,037e-5
Na	5,442e-1
Si	1,394e-4
pH	4,304

The next simulation consists of creating the initial heterogeneity pore water. As mentioned the start-out brine will be the one shown in table 4.5 for this step also. The graphics is shown below in figure 4.22.

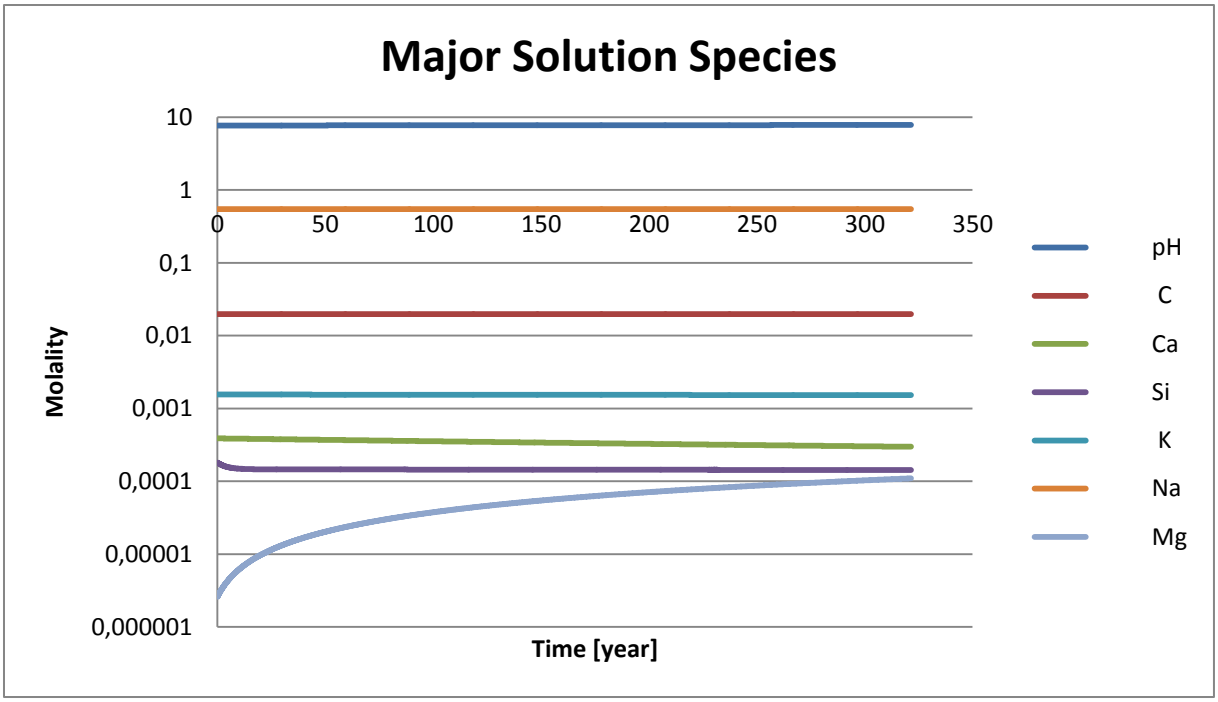

Figure 4.22: Pore water from (Audigane et al) equilibration process with heterogeneity sediment

Again one can see that the system is close to equilibrium after 300 years. And the endpoint numbers here are presented in table 4.7 below.

Table 4.7: Pore water to be present in heterogeneity.

Al	2,604e-8
C	1,966e-2
Ca	2,978e-4
Cl	5,375e-1
Fe	1,528e-6
K	1,528e-3
Mg	1,097e-4
Na	5,441e-1
Si	1,428e-4
pH	7,798

These will be the elements initially present in the heterogeneity.

4.1.4 Utsira Diffusive Transport

So first it will be attempted to investigate calcite dissolution in the same way as was done for Frio. This is to check if there are any similarities.

First, a digression on what will come in the next topic might be enlightening here. So in the next topic, after the Utsira results are presented, there will be a quick look on results from Frio where a type 2 infilling solution is used. This is done to show that the choice of infilling solution is going to be of great importance for the behavior of the system, even for very small timescales, as is the case in the present study. As will soon be revealed, similar behavior is seen in Utsira as was seen in Frio when type 1 infilling solutions were used. So looking at results where the infilling solution is changed to type 2 should be interesting for comparison.

The pH is shown in the figure 4.23 below.

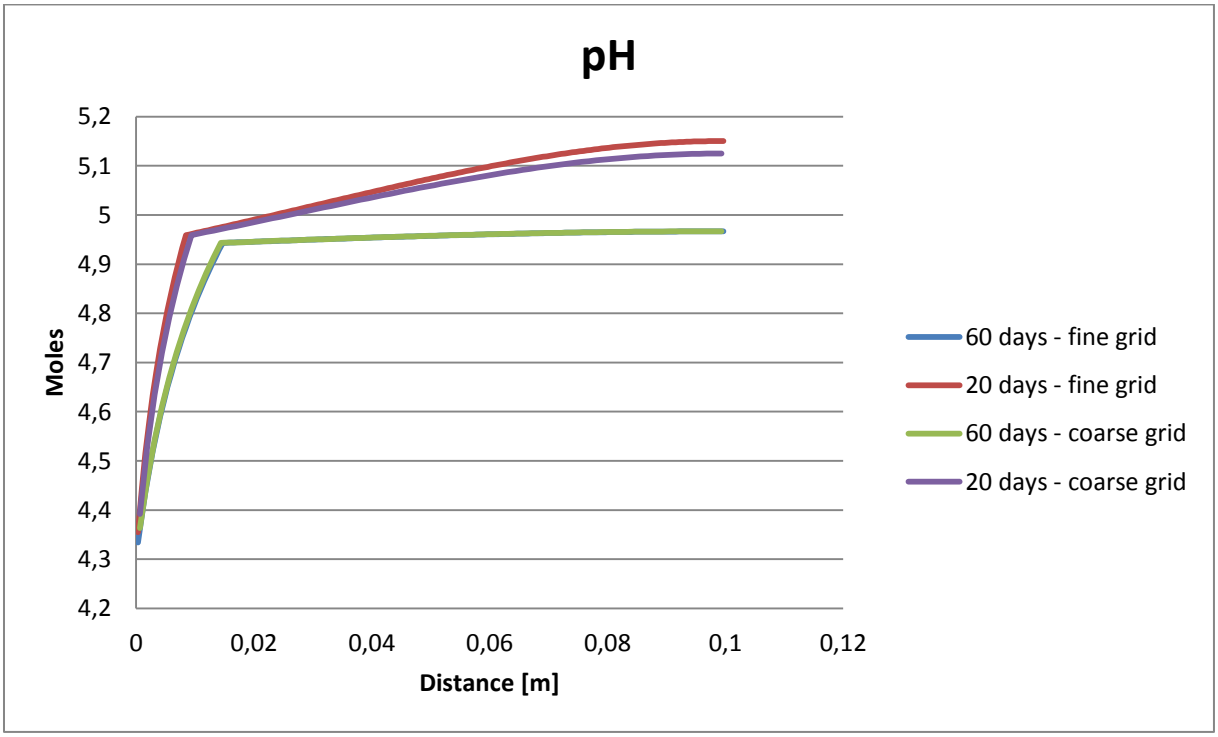

Figure 4.23: pH vs distance

The initial values for the infilling and the heterogeneity are found in table 4.6 and 4.7, respectively.

Further, calcite is shown in figure 4.24 below.

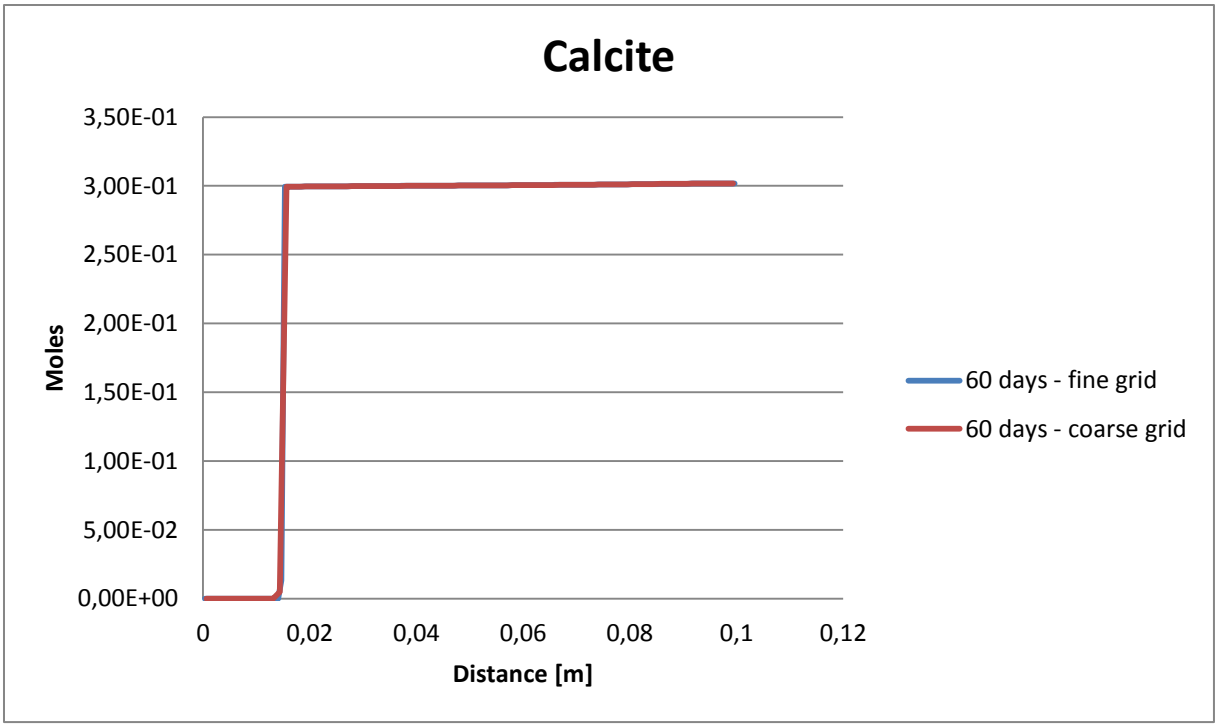

Figure 4.24: Calcite moles vs distance

As expected the same trend is found here as was found in the Frio simulation, with large calcite dissolution in the region close to the inlet, and only minor dissolutions otherwise. In this case there seems to be good correlations on the grid sensitivity though. A zoomed graphic showing that there has been some dissolution in the rest of the length is shown in figure 4.25.

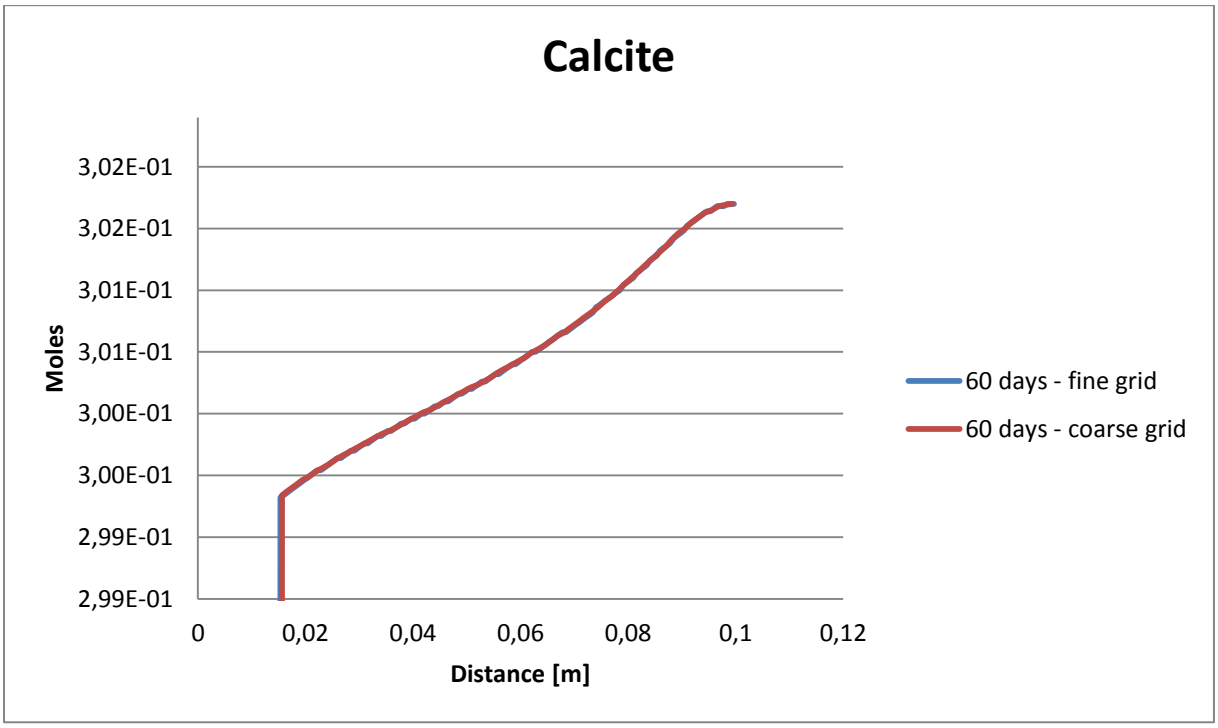

Figure 4.25: Calcite moles vs distance. This is a zoomed up graph to show the nuances.

The changes in the rest of the column is anticipated in this figure, but they are far smaller changes than the ones near the inlet.

A look at total calcium is shown in the following figure 4.26.

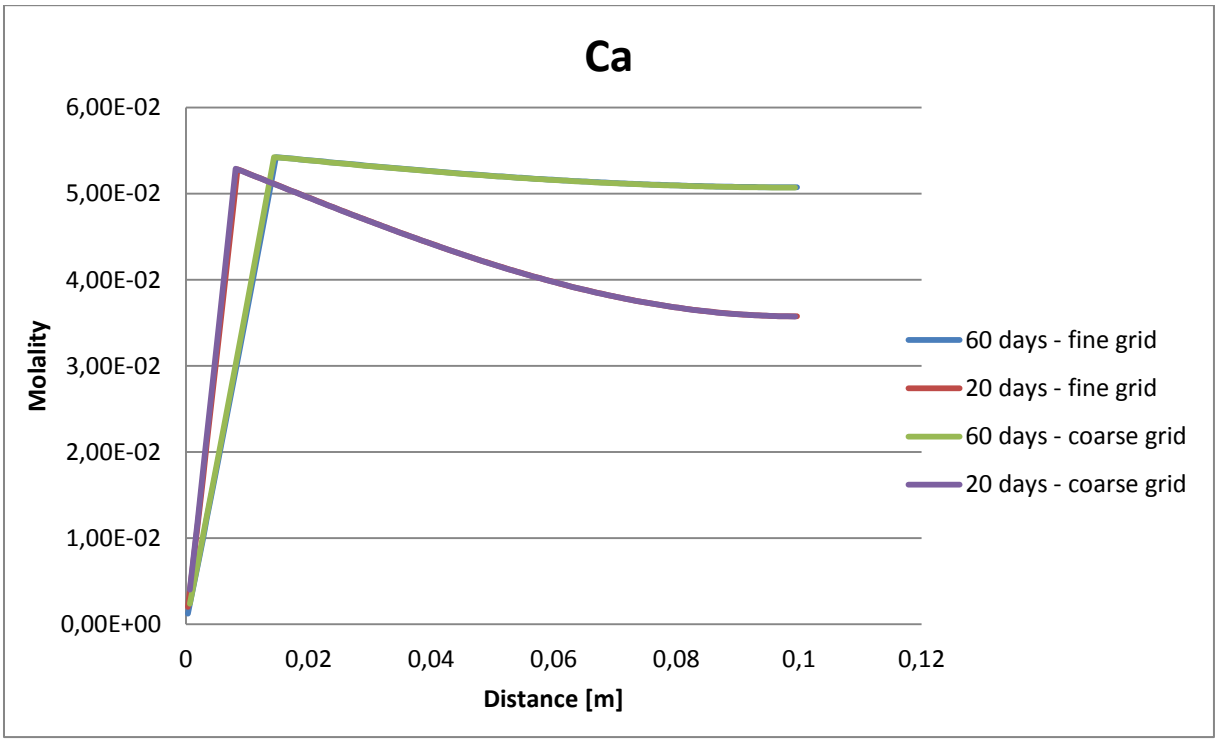

Figure 4.26: Calcium molality vs distance

The grid sensitivity reveals no numerical inaccuracy here. The initial molalities are available from the batch modeling results. The result here is very similar to that of Frio, with calcium diffusing out of the heterogeneity in seemingly large amounts.

Just as for Frio, there is presented results of the required time to dissolve individual cells. Again the maximum time is plotted, and the true answers are at most 2 days less than these. This is shown in figure 4.27.

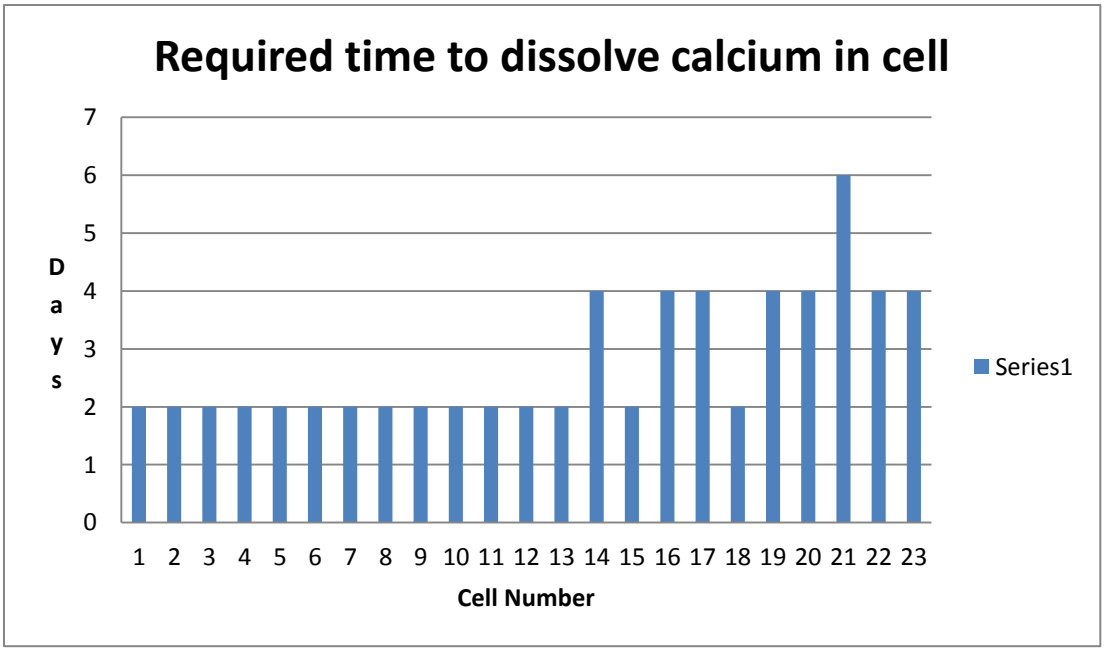

Figure 4.27: Time to dissolve total calcite in cell number. The time count starts when the previous cell has its calcium content dissolved.

The trend is clear this time also, but not as decisive as in the Frio case. Remember here again that one cell is the length of one 160^{th} of 10 cm. So the point made in the Frio section is here verified, namely that even very small increments in distance from the inlet solution makes a big difference with time, even after just 60 days. It is evident that the dissolution in the first cell takes probably far less than two days, and increasing with every cell, even though this is not visible near the inlet side with a resolution of two days.

Further, the difference from the Frio case is the number of cells dissolved after 60 days, more than three times as many. A quick look at the batch modeling reveals that both the pH and the total calcium is lower in the infilling Utsira brine than in the infilling Frio brine. Both of these factors are important in dissolving calcite. This should be a satisfying explanation for the larger calcite dissolution in Utsira. And as mentioned earlier there will be a type 2 infilling solution simulation for Frio after these Utsira results, just to check whether the large calcite dissolution will still be observed.

So just as for the Frio results, a study on dawsonite precipitation and where its aluminium is coming from follows. Dawsonite has been precipitated in small amounts, as was also the case in the Frio run. This can be seen I figure 4.28 that follows.

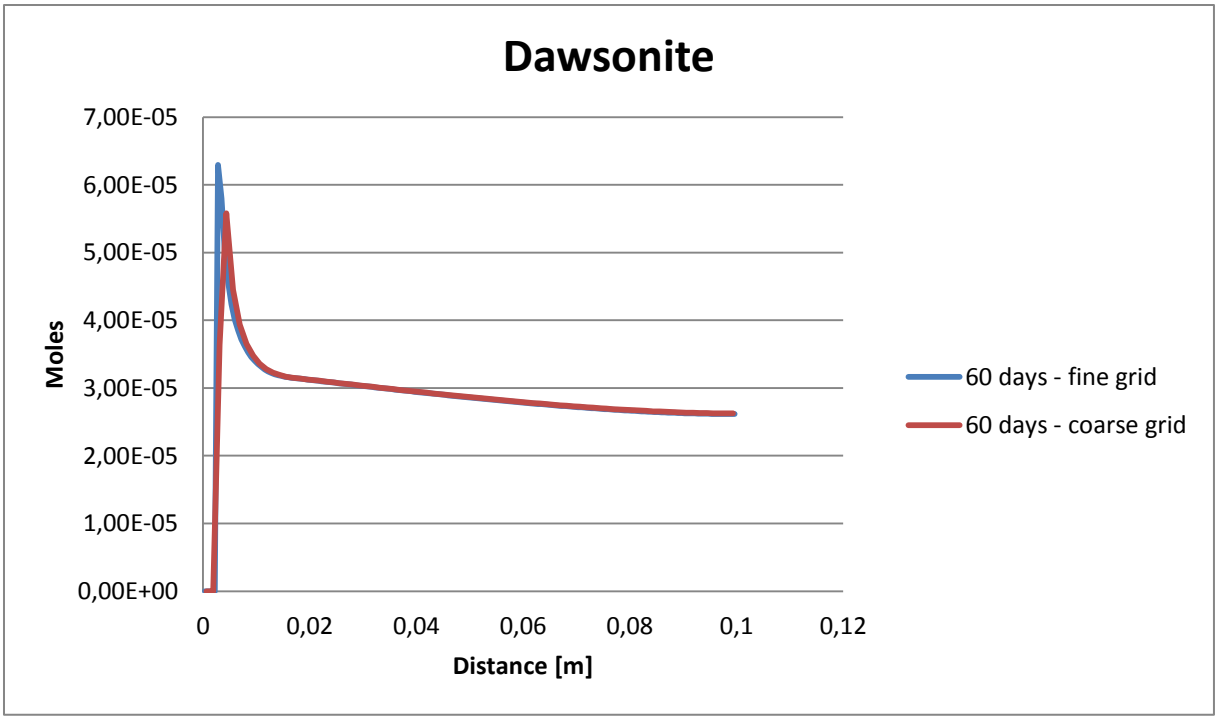

Figure 4.28: Dawsonite moles vs distance. Dawsonite is not present initially, and has been precipitated.

The trend is increasing dawsonite closer to the inlet, except for the first few cells where no dawsonite is present at all. Increasing amounts dawsonite towards the inlet was also the case in Frio, and was studied by looking at its elements. Most of the effort was devoted the study of al-containing minerals. The reason for this was the discovery that initially there was too small aluminium content to support the much higher dawsonite precipitation. By inspecting the initial aluminium content for Utsira, shown in figure 4.32, one can see that this is also the case here. For this reason, the minerals dissolving into aluminium products at non-trivial rates will also be studied here. These minerals include k-feldspar, albite and muscovite. As was the case for Frio, natrium is abundant, i.e. not too interesting for dawsonite precipitation. The other dawsonite complexes, carbonate and hydroxide are both at roughly the same abundance as in the Frio case. But as in the Frio section, these will not be studied any further here either. They are arbitrarily left out.

K feldspar is presented in the following figure 4.29.

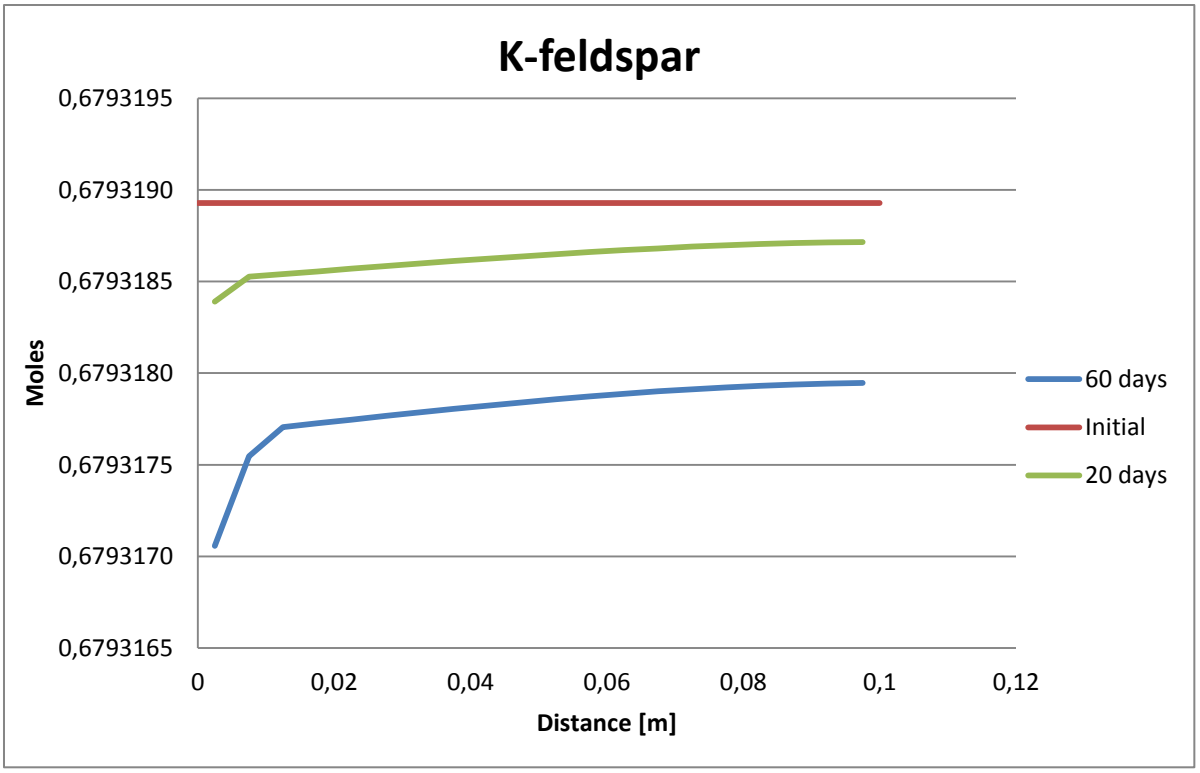

Figure 4.29: K-fedlspar moles vs distance. The first of the al-supplying minerals for dawsonite precipitation. There is no grid sensitivity for these minerals.

Here it seems like increased dissolution towards the inlet. And just as for Frio, the pH plot coincides strongly with the dissolution observed here, with reference to the dependence of proton activity in the rate equation E-1.

Further, a look on k-feldspars elements to continue the study on the reaction quotient in equation E-1, as was performed for Frio.

The first element of k-feldspar looked at is silicon, with reference to equation C-13. Silicon is presented in figure 4.30.

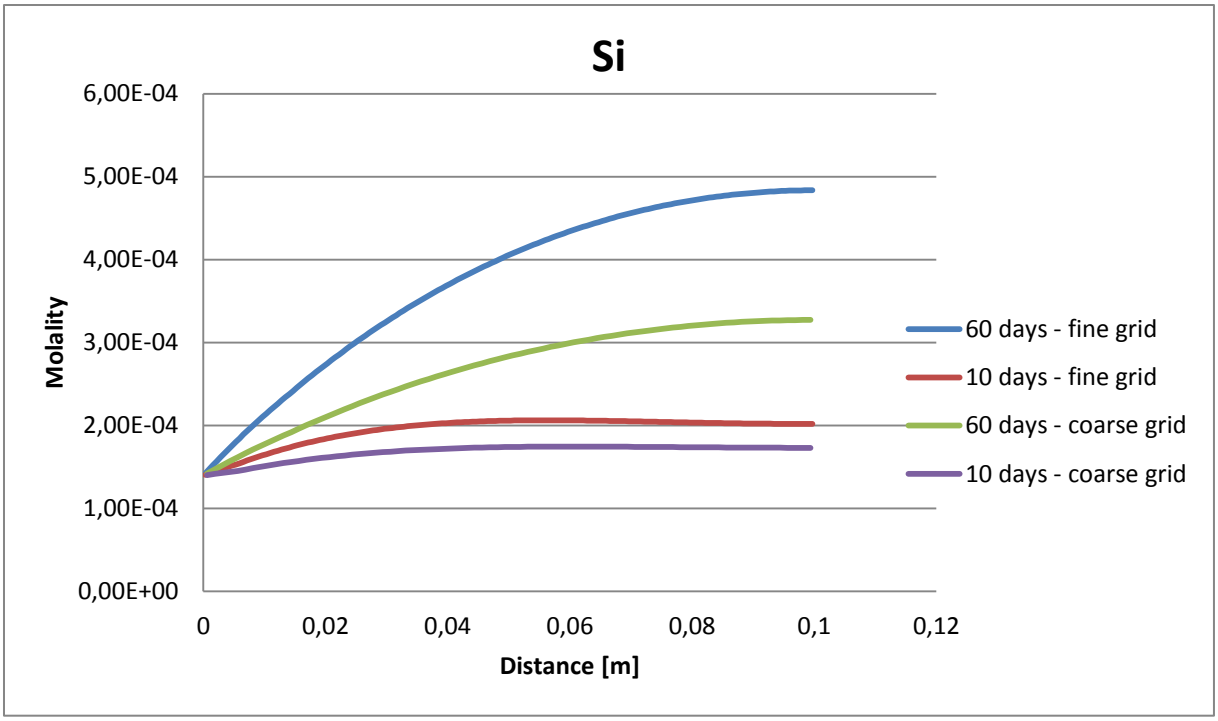

Figure 4.30: Silicon molality vs distance for various times.

The grid sensitivity is not perfect here. As is evident from the tables in the batch modeling, the initial amounts of silicon in the heterogeneity is just slightly larger than the amount in the infilling solution. However, many of the primary minerals that dissolve (though slow as always) contain silicon, so its abundance increases some with time. So silicon will generally be diffusing out of the heterogeneity. So here the concentration is decreasing closer to the inlet.

The next constituent of k-feldspar is potassium, presented in the following figure 4.31.

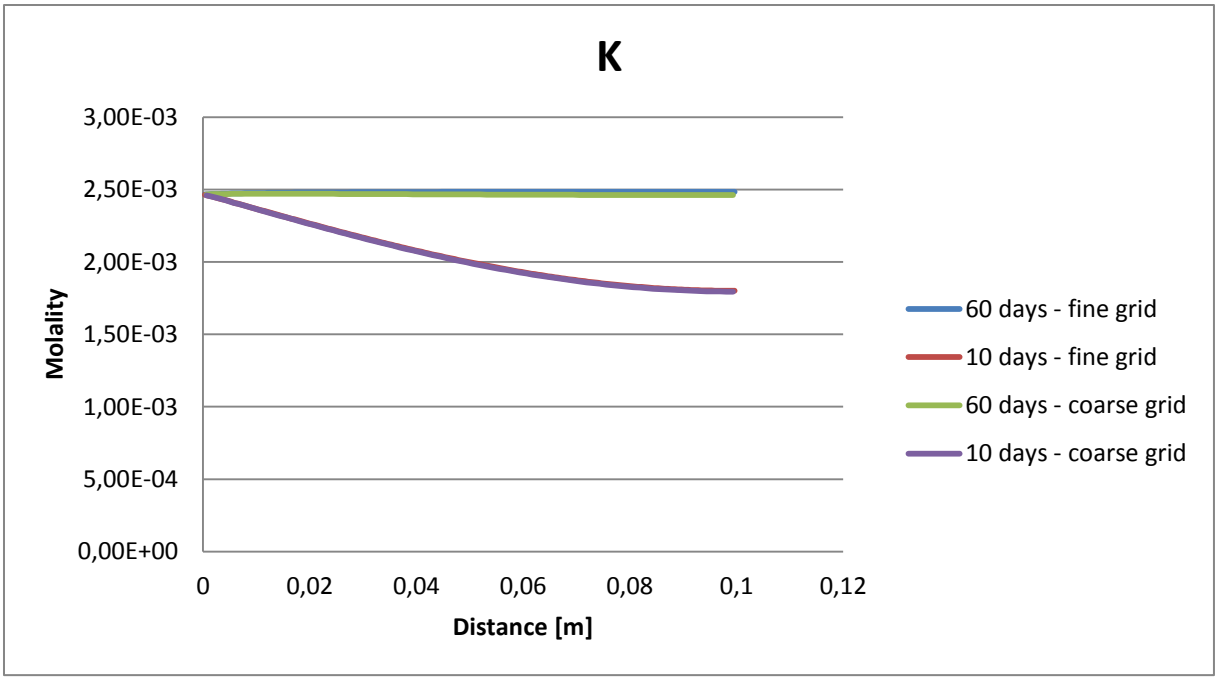

Figure 4.31: Potassium molality vs distance for various times

The grid sensitivity is satisfying here. The amount of potassium in the heterogeneity is just smaller than the amount in the infilling solution, so the profile looks consistent with potassium diffusing into the heterogeneity. This is in contrast to Frio where it was diffusing out of the heterogeneity. There is not much time before the concentration differences are equalized, but still it's not an instant process.

Further, a look at aluminium in Figure 4.32 below

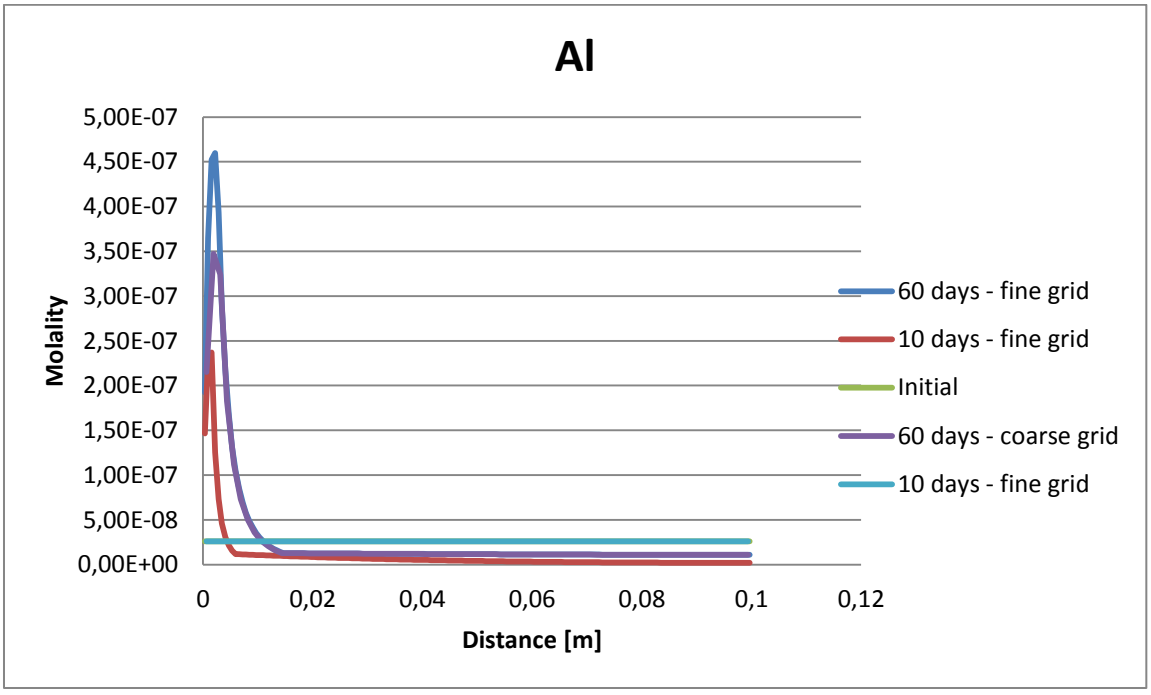

Figure 4.32: Aluminium molality vs distance for different times.

The grid sensitivity is not bad here either despite the low concentrations. Aluminium looks very similar to what it was in frio.

In summary, it is revealed that out of the k-feldspar elements, silicone, aluminum and potassium, only silicone shows decreasing concentrations towards the inlet end. So this weakens the faith in using the solution species concentrations profiles to predict mineral dissolution through the reaction quotient.

The next mineral is albite, with its elements shown in equation C-11. Albite is shown in figure 4.33 below.

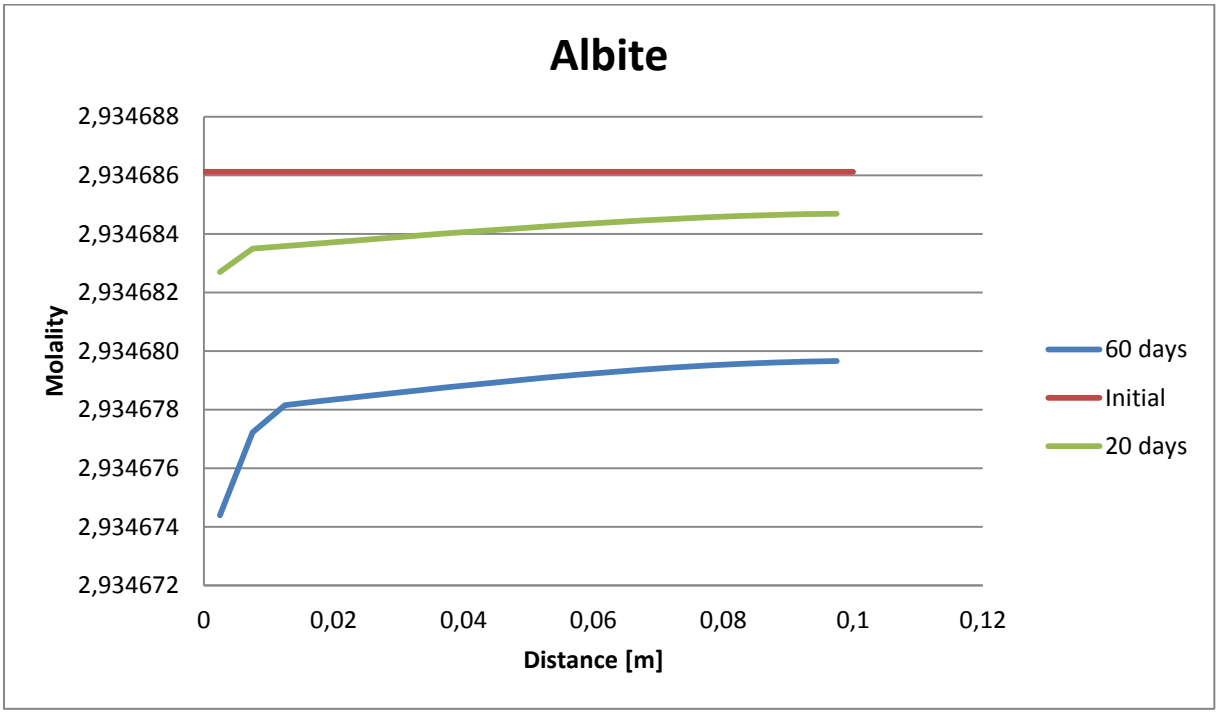

Figure 4.33: Albite moles vs distance. Albite is the second al-supplying mineral for dawsonite precipitation.

The same dissolution trend as for the other minerals are again revealed. The proton activity is again strengthened as seemingly largest contributor to the dissolution rates.

Further, the new element to study here is natrium, which is presented in figure 4.34.

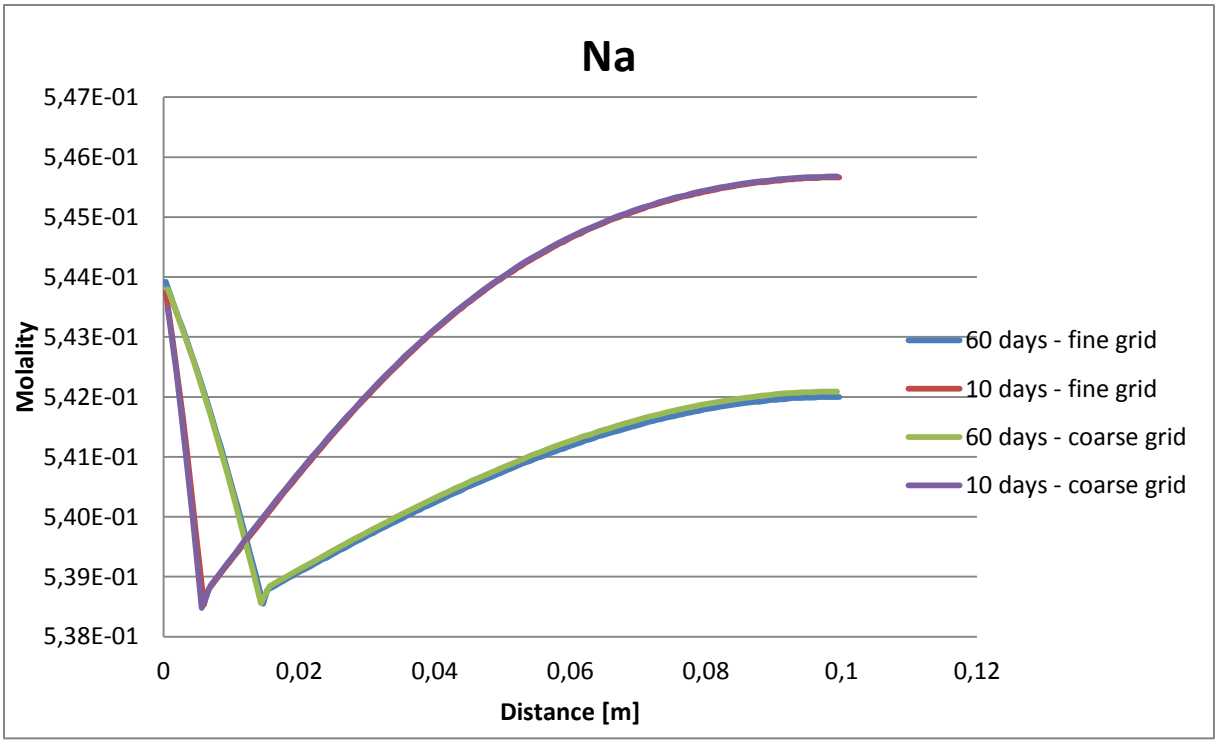

Figure 4.34: Natrium molality vs distance for various times.

The grid sensitivity is pretty accurate. The natrium concentration is initially very close in the infilling solution and the heterogeneity in this case, both similar to the leftmost concentration in the figure. Natrium generally seems to be consumed in the heterogeneity, but with a faster rate towards the inlet. In the first cells, however, there is an abrupt jump in concentration due to diffusion from the infilling solution.

Albite consists of natrium, aluminium and silicone. So from the natrium curve one can't really say much in regards to the reaction quotient. It does in fact have the decreasing trend towards the inlet, but suddenly there is a large jump. Only the decrease is consistent with the ablite dissolution (with regards to the superficial analysis applied here). So one can't really say too much on this matter.

So proceeding with muscovite, shown in figure 4.35.

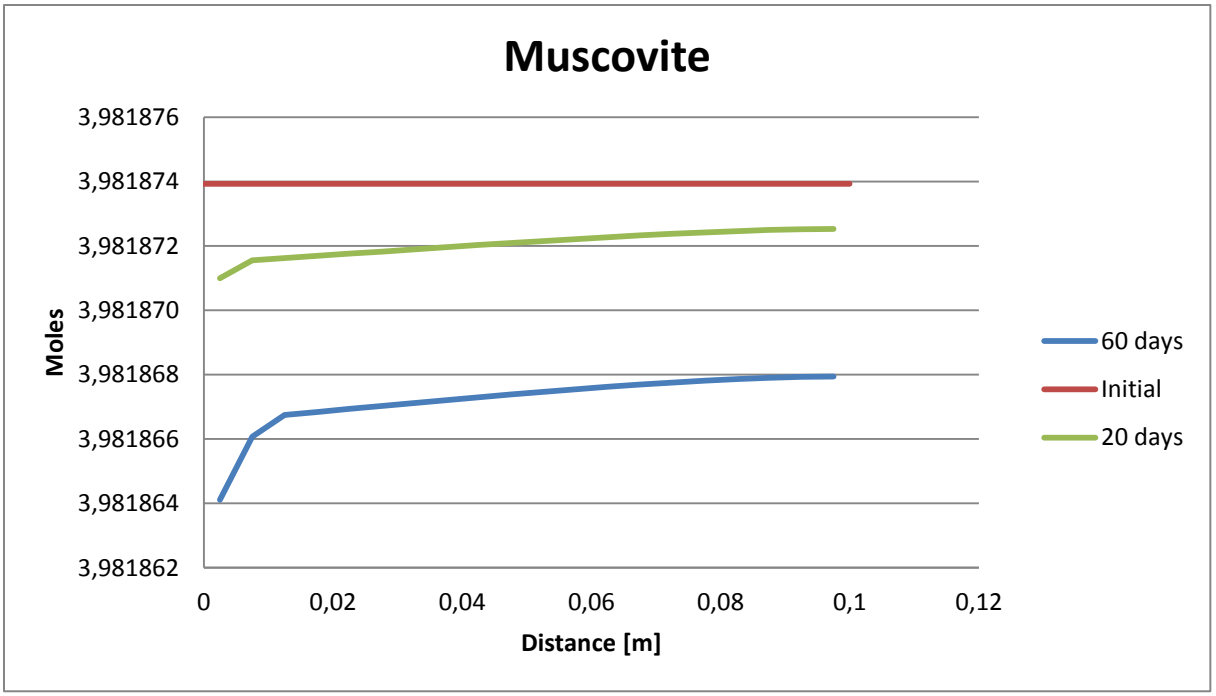

Figure 4.35: Muscovite moles vs distance. Muscovite is the third al-supplying mineral for dawsonite precipitation.

The trend is as always the increased dissolution towards the inlet side with an abrupt increase in the first cells, consistent with the pH.

The elements interesting for muscovite can be seen in equation C-26 to be potassium, aluminium and silicone. Of these only the decreasing potassium is consistent with mineral dissolution towards the inlet, again with singlehandedly respect to the reaction quotient.

So also in this Utsira run the pH seems to be the single most important factor on the dissolution rates. All of the al-minerals graphs coincide with the pH, which one therefore should expect to be highly correlated to the proton activity in equation E-1.

But when studying the reaction quotient for Utsira, with the assumption that concentrations are closely related to activities, it is revealed a very poor correlation. There really seems to be no system in this for this Utsira run, whereas in Frio there could seem to be at least some correlation.

So it's possible that the proton activity is just a too strong factor so that the reaction quotient becomes trivial. Or it could be a bad approach assuming concentrations correspond well to activites. Also, there wasn't performed an analysis of all the species in every mineral, like e.g. hydroxide or carbonate.

There is one case, though, where both the reaction quotient as well as the pH is obviously important, and that is in the large dissolution observed, described in the calcite discussion.

4.1.5 Frio batch modeling (part 2: type 2 infilling solution)

Now that the results from Frio and Utsira are presented, there will be a look at a simulation of Frio, but where a type 2 infilling solution is used instead of a type 1. As mentioned, the change here will be that the infilling solution is allowed to be equilibrated with both the sandstone sediment and the gaseous CO_2 phase, as opposed to the CO_2 phase alone. This will cause both the pH and the calcium content to be larger in the infilling solution, and will be shown soon.

The reason this whole simulation is performed is merely to support the discussion on the large calcite dissolution observed in both Frio and Utsira. The reason behind this dissolution was believed to be the ability of the infilling solution to both serve protons into the heterogeneity and drain out the calcium in large amounts due to the concentration difference. So now that these differences will be smaller, one can check whether they really matter that much.

The pore water in the heterogeneity is going to be equal to what it was in the Frio simulation. This was previously presented in figure 4.4.

Further, the creation process of the infilling solution is going to be as follows. The sandstone pore water taken from the source study (Xu et al 2005) is again taken as the start-out brine. This is then equilibrated with the sandstone system and data used in the present study. This was also the first steps done in the first Frio batch modeling, and the result was presented in figure 4.1. The continuation will here be to let this system react with CO_2 and the sandstone sediment together for an arbitrary chosen amount of time equal to 18 years. The end results from this simulation is presented in table 4.8.

Table 4.8: Carbonated sandstone brine (infilling solution type 2)

Al	7,211e-9
C	1,371
Ca	5,198e-2
Cl	1,001
Fe	1,879e-13
K	7,766e-3
Mg	1,341e-4
Na	9,788e-1
Si	2,779e-3
S	1,321e-9
pH	4,918

If one compares the carbonated brine for the first Frio run, table 4.2 with this one, table 4.8, one can see that the pH is roughly 0,5 larger now, and the calcium content nearly 50 times

larger. This is because the sediment (which includes calcite) is considered reactive in this last run, whereas it was kept unreactive in the previous run.

4.1.6 Frio Diffusive Transport (part 2: type 2 infilling solution)

The results for calcite is presented in figure 4.36.

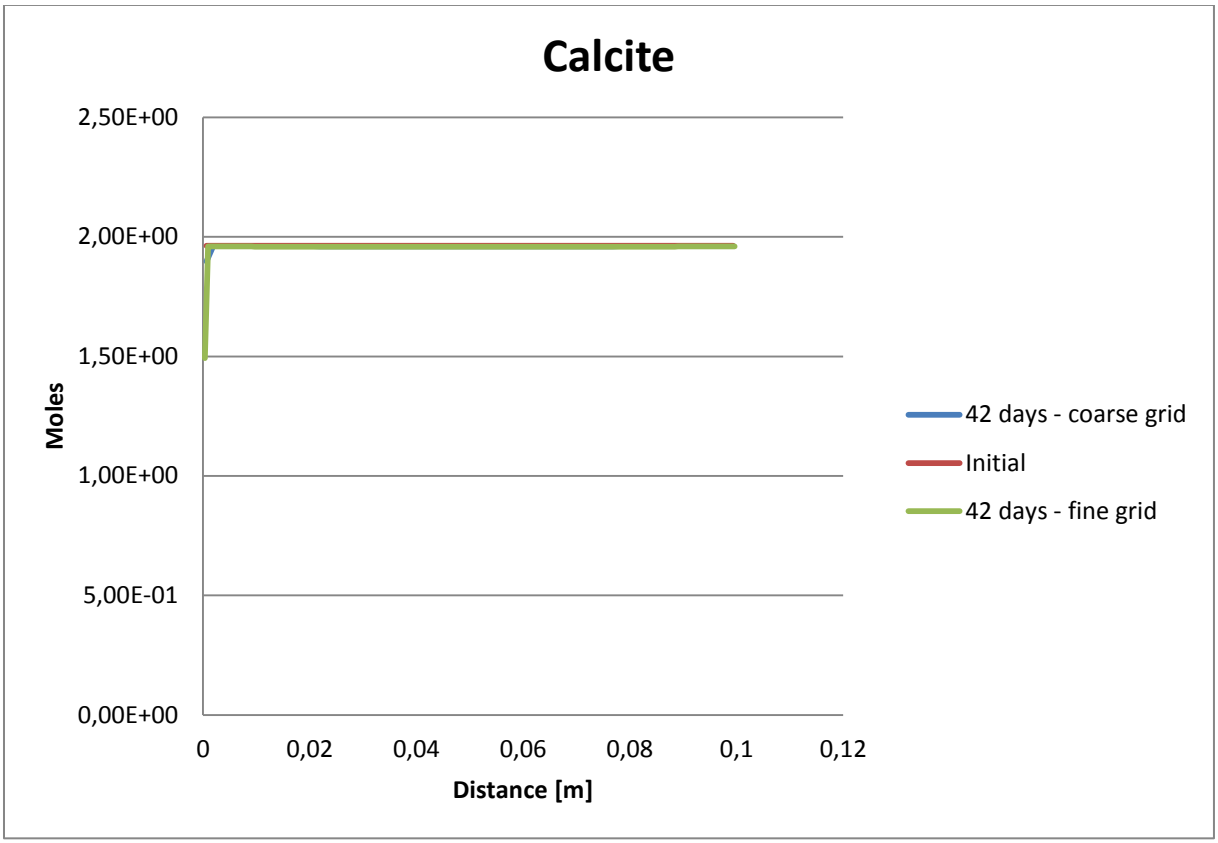

Figure 4.36: Calcite moles vs distance after 42 days.

The simulation was run for 42 days only. No more time is needed since this is only to check whether the calcite dissolution trend is found here also. As one can see, the result is quite different from both the Frio and the Utsira cases presented earlier. None of the first cells have been fully dissolved of its calcite content, and only the first cell shows an interesting change. The similarity to the previous runs is that the calcite dissolution appears to be stepwise here also, dissolving one cell before the next cell is taken upon.

A note on the infilling solution. The type 2 solution was created assuming reactions between CO_2 gas phase – brine – and sediment for 16 years, but the results wouldn't have changed much if even a far smaller amount of time was used here. The reason is that the calcite is assumed to be an equilibrium reactant, i.e. always in equilibrium with the brine. So the largest changes happened the instant the brine was allowed to react with the sediment. The calcium content increased significantly at this instant, and only smaller changes are made through the rest of the 16 years. So the amount of years used here is not really important.

Further, as one can see from figure 4.7, the first 7-8 cells have had about 10 moles calcite dissolve, supplying the same amount of calcium into solution. This calcium should be traceable, but at the end of the simulation, almost nothing remains. The size of the solutions in any grid cell, including the infilling solution is one 160^{th} liter. Most of this have been diffusing out because of the boundary condition chosen. As mentioned, constant concentration means that the infilling solution will be updated to its initial content for every time step calculated. So if the solution just inside the heterogeneity is close to saturated in calcium, and the infilling solution is not, there will be a significant amount of calcium diffusion out for every time step. This is the type1 infilling solution runs.

Now if both the infilling solution and the solution just inside the heterogeneity is close to saturated in calcium, there will only be small amounts diffusing in or out each time step. So this was the case run in these last result obtained, and as one can see far smaller amounts of calcite is dissolved.

So this means that when running these PHREEQC simulations it's going to be important to use an infilling solution that does what one wants it to do throughout the simulation. There are two important points here. The first is that the infilling solution must be made so that it represents exactly what one wants to model. And the second is the adequate choice of boundary conditions.

5 FURTHER WORK

Here is presented a small introduction to stylolites, and proposed how this could be a scenario in a similar study as the present.

Pressure solution is a geochemical process where mineral dissolution is provoked in regions of high stress (Ebner et al 2009). Increased stress implies increased strain and deformation, which is believed to cause increased mineral solubility (Barton and Parnell 2007). The minerals removed are mostly calcite and quartz (Peackock and Azzam 2006). The areas of increased stress are at the grain contacts. The dissolved material may precipitate in pores nearby, reducing the porosity. The produces a seam of insoluble residues in close contact between grains (Abner et al 2009). So the resulting picture will be some zones where higher dissolution has occurred, and some zones where higher cementation due to the precipitated material has occurred (Dewers 1994).

Stylolite formation is believed to be affected by many factors, including temperature, pressure, mineralogy and more. There is however no general consensus on the importance of each factor (Barton and Parnell 2007).

The effect of carbonated brine on stylolite minerals dissolution and precipitation could be studied as in the following figure 4.37.

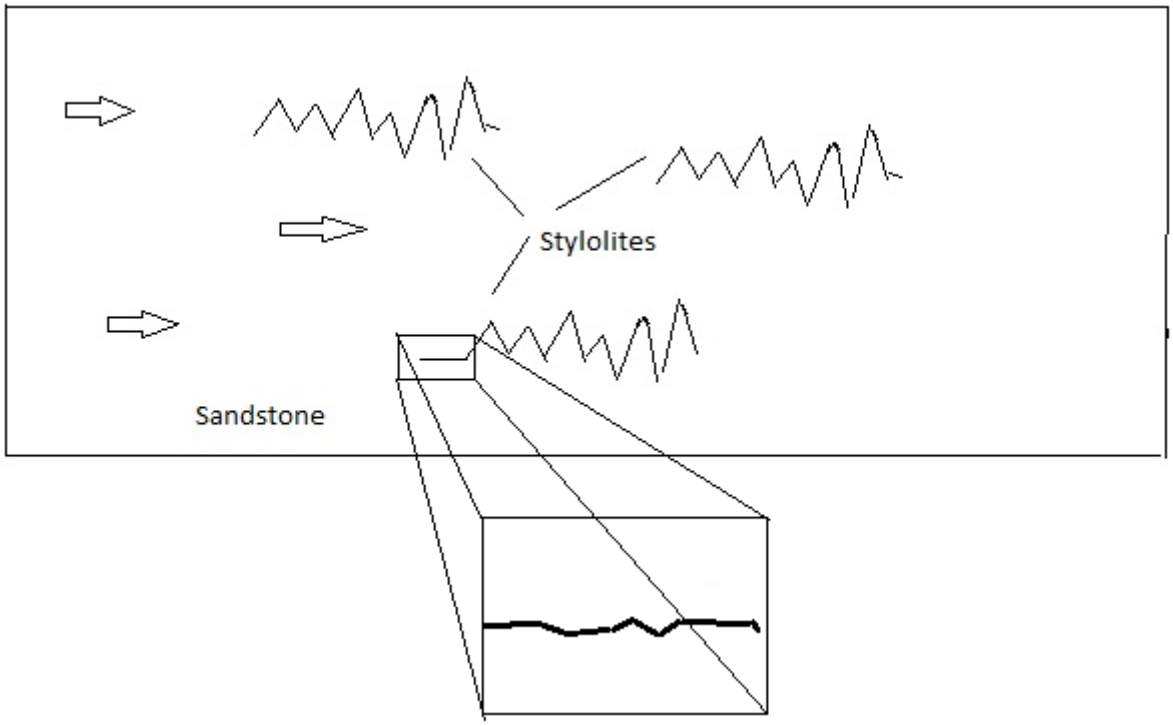

Figure 4.37: A heterogeneity scenario of a stylolite in a sandstone reservoir. This might be studied as further work.

The figure shows a rough sketch of how stylolites may be present in a sandstone reservoir. Since it's only the reaction mechanisms that are interesting, only a small part of a stylolite is modeled, as highlighted in the figure. Also, recall that PHREEQC models transport in only 1D, so it is assumed that the small part of the stylolite modeled is completely straight and not slightly serrated like in the highlighted part of the figure.

As other possibilities for further work, one could perform sensitivities on the rate equation proton activity exponent, n, from equation E-1. And mineral reactive surface areas are very uncertain, calling for sensitivities. Of course what the present study lacks is larger timescales, only 60 days are simulated here. So this is probably the most important variable.

Also important, and very uncertain, is the secondary minerals. .Also there are plenty of other alternatives, e.g kinetic rates are uncertain and mineral compositions are uncertain. All of these variables have been discusses in the theory sections.

But as mentioned earlier, boundary conditions could be run with for example flux, with any chosen volume of the infilling solution. And of course there are many options in creating the infilling solution, so also here sensitivities could be performed.

As a last mention one could simulate different sites than Frio and Utsira.

6 CONCLUSIONS

- There is revealed that the choice of infilling solution and boundary conditions are highly important for the mass transport in the system. This is manifested in the simulation results through large calcite dissolution near the inlet.
- The large calcite dissolution observed in both Frio and Utsira is induced by the diffusive removal of calcium and the pH lowering.
- The large dissolution rate of calcite decreases drastically by tiny increments in distance from the inlet.
- The calcite dissolution was in 60 days > three times further intruded into the heterogeneity in Utsira than in Frio. The reason was revealed to be the lower calcium concentration and pH in the Utsira infilling solution.
- Dawsonite precipitated in both the Frio and the Utsira run, but in small amounts.
- The aluminium for dawsonite precipitation is provided through dissolution of five minerals in Frio and three in Utsira.
- The dissolution rate of these minerals is highly correlated with the pH, showing a jump in dissolution rate close to the inlet, then a slow decrease through the rest of the heterogeneity. This was the case for both Frio and Utsira.
- There seems to be very small merit in predicting the dissolution rate through the reaction quotient in equation E-1, by looking at individual species concentration profiles. The far better predictor is the pH profile.
- The additional Frio run revealed that changing the infilling solution to a brine somewhat equilibrated by both CO_2 and sediment, as opposed to CO_2 alone where the sediment is kept unreactive, hindered the large calcite dissolution from happening.
- This was showed to be because the infilling solution in this case has a much larger calcium concentration, thereby reducing the diffusion of calcium from the heterogeneity by a large amount since the concentration difference is smaller.
- This last result here also shows that the reaction quotient is far more important than the pH in this particular case, not allowing calcite to dissolve due to high calcium concentration.

7 REFERENCES

Appelo, C.A.J., Postma, D., 2005. Geochemistry, Groundwater and Pollution. 2nd edn. Balkema, Leiden. 649 pp. ISBN 978-0415364287.

Audigane, P., Gaus, I., Pruess, K., Xu, T. 2006. A Long Term 2D Modelling Study of CO_2 Storage at Sleipner (North Sea) Using Toughreact. Proceedings in TOUGH Symposium, San Francisco, USA, 12-22 May.

Barton, M., Parnell, J. 2007. Relationshits between stylolites and cementation in sandstone r eservoir: Examples from the Northe Sea, U.K. and East Greenland: Sedimentary Geology 194, 17-35.

Dewers, T., Ortoleva, P., 1994. Formation of stylolites, Marl/Limestone alternations, and dissolution (clay) seams by unstable chemical compaction of argillaceous carbonates: Developments in sedimentology 51.

Dickson, A.G.and Goyet, C. 1994. Handbook of methods for the analysis of the various parameters of the carbon dioxide system in sea water. Version 2, eds. ORNL/CDIAC-74.

Ebner, M., Koehn, D., Toussaint, R., Renard, F., 2009. The influence of rock heterogeneity on the scaling properties of simulated and natural stylolites: Journal of Structural Geology 31, 72-82.

Flett, M., Gurton, R., Weir, G., 2007. Heterogeneous saline formations for carbon dioxide disposal: impact of varying heterogeneity on containment and trapping. Journal of Petroleum Science and Engineering 57, 106-118.

Gaus, I., Azaroual, M., Czernichowski-Lauriol, I., 2005, Reactive transport modelling of the impact of CO2 injection on the clayey cap rock at Sleipner (North Sea). Chemical Geology 217, 319-337.

Iglesias, R., Ketzer, J.M., Einloft, S., Dullius, R., Ligabue., Lima, V.de., 2009. Water-rock-CO2 interactions in saline aquifers aimed for carbon dioxide storage: Experimental and numerical modeling studies of the Rio Bonito Formation (Permian), southern Brazil; Applied Geochemistry 24, 760-767.

Intergovernmental Panel on Climate Change (IPCC). 2005. Special report on carbon dioxide capture and storage. Prepared by Working Group III of the IPCC, Cambridge University Press, Cambridge, U.K.

Liu, F., Lu, P., Zhu, C., Xiao, Y., 2011. Coupled reactive flow and transport modeling of CO2 sequestration in Mt. Simon sandstone formation, Midwest U.S.A.

Marini, L., 2006. Geological Sequestration of Carbon Dioxide, Volume 11: Thermodynamics, Kinetics, and Reaction Path Modelling. 11 edn. Elsevier Science. 470 pages. ISBN 978-044529503.

Michael, K., Golab, A., Shulakova, V., Ennis-King, J., Allison, G., Sharma, S., Aiken, S., 2010. Geological storage of CO2 in saline aquifers – A review of the experience from existing operations.

Palandri, J.L., Kharaka, Y.K., 2004. A compilation of Rate parameters of water-mineral interaction kinetics for application to geochemical modeling. U.S Geological survey. Open file report 2004-1068.

Parkhurst, D.L. and Appelo, C.A.J., 1999. Users guide to PHREEQC (version 2) – A computer program for speciation, batch-reaction, one-dimensional transport, and inverse geochemical calculations: U.S Geological Survey Water-Resources Investigations Report 99-4259,312p.

Peacock, D.C.P., Azzam, I.N., 2006. Development and scaling relationships of a stylolite population: Journal of Structural Geology 28, 1883-1889.

Pearce, J.M., Kemp, S.J., Wetton, P.D., 1999. Mineralogical and petrographical characterization of 1m core from the Utsira formation, Central North Sea: British Geological Survey, Report WG/99/24C.

Rahimpour-Bonab, H., 2007. A procedure for appraisal of a hydrocarbon reservoir continuity and quantification of its heterogeneity: Journal of Petroleum Science and Engineering 58, 1-12.

Shukla, R., Ranjith, P., Haque, A., Choi., X., 2010. A review of studied on CO2 sequestration and caprock integrity. Fuel 89, 2651-2664.

Sonnethal, E.L., Spycher, N., 2001. Drift-Scale coupled processes (DST and THC seep-age) models. AMR N0120/U0110 Rev.01, Yucca Mountain Project, Lawrence Berkeley National Laboratory, Berkley, California.

Soong, Y., Jones, J.R., Harrison, D.K., Hedges, S.W., Goodman, A.L., Baltrus, J.P.,2003. Mineral trapping of CO2 with Oriskany brine: Fuel chemistry division preprints, 48(1), 119.

Xu, T., Apps, J.A., Pruess, K., . 2005. Mineral sequestration of a sandstone-shale system: Chemical geology, v. 217, (3-4), p. 295-318.

Xu, T., Zheng, L., Tian, Hailong., 2011. Reactive transport modeling for CO2 geoological sequestration: Journal of Petroleum Science and Engineering 78, 765-777